Effects of Asymmetric Latent Heating on Typhoon Movement Crossing Taiwan: The Case of Morakot (2009) with Extreme Rainfall

CHUNG-CHIEH WANG,* HUNG-CHI KUO,+ YU-HAN CHEN,* HSIAO-LING HUANG,+ CHAO-HSUAN CHUNG,* AND KAZUHISA TSUBOKI#

* *Department of Earth Sciences, National Taiwan Normal University, Taipei, Taiwan*
+ *Department of Atmospheric Sciences, National Taiwan University, Taipei, Taiwan*
# *Hydrospheric Atmospheric Research Center, Nagoya University, Nagoya, Japan*

(Manuscript received 26 December 2011, in final form 4 July 2012)

ABSTRACT

Typhoon Morakot struck Taiwan during 6–9 August 2009, and it produced the highest rainfall (approaching 3000 mm) and caused the worst damage in the past 50 yr. Typhoon–monsoon flow interactions with mesoscale convection, the water vapor supply by the monsoon flow, and the slow moving speed of the storm are the main reasons for the record-breaking precipitation. Analysis of the typhoon track reveals that the steering flow, although indeed slow, still exceeded the typhoon moving speed by approximately 5 km h^{-1} (1 km h^{-1} = 0.28 m s^{-1}) during the postlandfall period on 8 August, when the rainfall was the heaviest. The Cloud-Resolving Storm Simulator (CReSS) is used to study the dynamics of the slow storm motion toward the north-northwest upon leaving Taiwan. The control simulations with 3-km grid size compare favorably with the observations, including the track, slow speed, asymmetric precipitation pattern, mesoscale convection, and rainfall distribution over Taiwan. Sensitivity tests with reduced moisture content reveal that not only did the model rainfall decrease but also the typhoon translation speed increased. Specifically, the simulations consistently show a discernible impact on storm motion by as much as 50%, as the storms with full moisture move slower (~5 km h^{-1}), while those with limited moisture (≤25%) move faster (~10 km h^{-1}). Thus, in addition to a weak steering flow, the prolonged asymmetric precipitation in Typhoon Morakot also contributed to its very slow motion upon leaving Taiwan, and both lengthened the heavy-rainfall period and increased the total rainfall amount. The implications of a realistic representation of cloud microphysics from the standpoint of tropical cyclone track forecasts are also briefly discussed.

1. Introduction

Typhoon (TY) Morakot (TY0908) during 7–9 August 2009 (Fig. 1) was the most devastating typhoon to strike Taiwan in recorded history, with a death toll of 757 and direct damages over $110 billion [New Taiwan dollars (NT$); ~$3.8 billion (U.S. dollars); Chanson 2010; http://www.hurricanescience.org]. Being merely an intermediate tropical cyclone (TC) in core intensity (category 2 on the Saffir–Simpson scale), Morakot did its destruction almost entirely due to the extreme rainfall that reached 2855 mm (over 4 days) rather than high winds (e.g., Hendricks et al. 2011). The record-breaking rainfall caused flooding over nearly the entire southwestern plain and triggered numerous mudslides over the mountains, where the tragic burying of Shiao-lin Village on the morning of 9 August alone took nearly 660 lives (Figs. 2a,b).

In the aftermath of Morakot, the National Science Council (NSC) of Taiwan organized an investigation into this event. The preliminary report (Hsu et al. 2010) and some other recent works listed several factors that collectively contributed to the unprecedented, extreme heavy rainfall during the period. These factors, some quite unique or at least unusual, include the large-scale monsoon gyre in which Morakot was embedded (e.g., Hong et al. 2010; Ge et al. 2010; Nguyen and Chen 2011); a large TC size with strong outer circulation (e.g., Jou et al. 2010); the slow translation speed near Taiwan (e.g., Hong et al. 2010; Chien and Kuo 2011; Wu et al. 2011; cf. Fig. 1); the strong low-level moisture flux from the southwest and asymmetric rainfall distribution (e.g., Chen et al. 2010; Kuo et al. 2010; Chien and Kuo 2011;

Corresponding author address: Prof. Chung-Chieh Wang, Department of Earth Sciences, National Taiwan Normal University, No. 88, Sec. 4, Tingzhou Rd., Taipei 11677, Taiwan.
E-mail: cwang@ntnu.edu.tw

DOI: 10.1175/JAS-D-11-0346.1

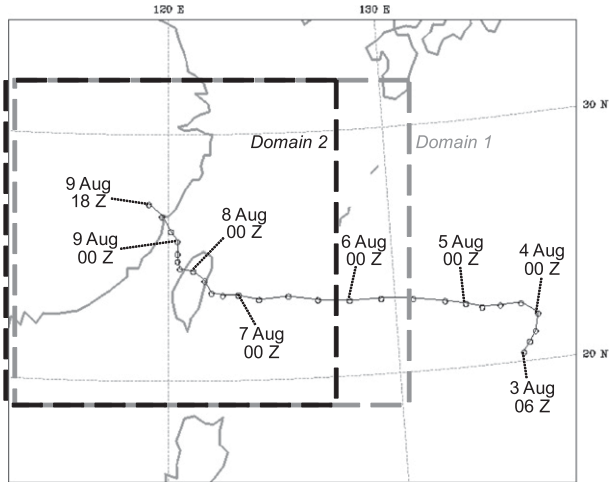

FIG. 1. JTWC track of Typhoon Morakot (2009) and the two domains used in this study. Locations of the TC center are indicated by open circles each 6 h, and the dates are given at 0000 UTC and at the end points.

Hendricks et al. 2011; Liang et al. 2011); the large moisture flux convergence and repeated formation of slow-moving rainbands just upstream from southern Taiwan (e.g., Chen et al. 2010; Kuo et al. 2010); and the rainfall enhancement by the steep topography of Taiwan (e.g., Ge et al. 2010; Hong et al. 2010; Wu et al. 2011; Fang et al. 2011). All of these factors contributed to the heavy rainfall for a lengthy period and consequently the extreme rainfall accumulation (e.g., Jou et al. 2010; cf. Fig. 2). Obviously, many of these factors are interrelated with complex and nonlinear interactions. The focus of this study is mainly on the linkages and feedbacks between the slow translation speed and asymmetric rainfall pattern, specifically during the postlandfall and heavy-rainfall period on 8 August (cf. Figs. 1, 2).

Hong et al. (2010) examined the large-scale environment of Morakot and concluded that a monsoon gyre, with a period of 10–30 days and about 4000 km in size, propagated from the southeast toward the northwest across the western North Pacific (WNP) in early August 2009 (their Figs. 3b–e). Thus, Morakot was subjected to an easterly background flow when it approached Taiwan on 5 August, but a relatively weak ambient flow occurred near its landfall in Taiwan on 8 August. Similarly, Ge et al. (2010), Wu et al. (2011), and Liang et al. (2011) suggest that the early westward track and then a nearly 90° turn northward over 5–10 August (cf. Fig. 1) were mainly determined by the interaction of Morakot's circulation with its larger-scale background. Recently, Chien and Kuo (2011) analyzed the mean flow associated with Morakot and discussed the role of a weakened steering flow in leading to the extreme rainfall. Later in section 4b, their results will be compared with ours.

Clearly, the unusually slow translation speed of Morakot was a crucial key factor (Jou et al. 2010; Chien and Kuo 2011; Wu et al. 2011), especially on 8 August (in UTC) when it was over the northern Taiwan Strait (only about 5.4 km h^{-1}, 1 km h^{-1} = 0.28 m s^{-1}; Fig. 1). During this period, the rainfall intensity over southern Taiwan was at a maximum (Fig. 2b). Chien and Kuo (2011) examined the relationship between rainfall, translation speed, and TC intensity during both landfall and postlandfall periods in 52 landfalling typhoons in Taiwan from 1977 to 2009. Here, the landfall period refers to the time when the TC center is over Taiwan, and the postlandfall period is defined as the interval for a TC to leave Taiwan until 100 km offshore. They found that the typhoon-induced total rainfall [summed over 25 Central Weather Bureau (CWB) surface stations] is more related to the TC translation speed (with an inverse relationship, i.e., slower-moving TCs bring more rain) rather than intensity, and the excessive rain of Morakot occurred during the postlandfall period (Chien and Kuo 2011, their Figs. 3 and 4). Considering the 18 strong rainfall (≥2000 mm, summed over 25 stations) typhoons from the dataset of Chien and Kuo (2011), Morakot was among the slowest TCs (lower left in Fig. 3a) during both landfall and postlandfall periods (with the same definitions), especially the latter (cf. Fig. 1). During its postlandfall period, Morakot produced far more rain than during the landfall period and surpassed all other TCs since 1977 (Fig. 3b). Thus, the reason for the very slow motion of Morakot after leaving Taiwan is of great importance from the standpoint of both science and hazard reduction.

Another important feature of Morakot (2009) was its asymmetric rainfall distribution (Fig. 4), which is linked to the strong moisture supply from the southwest (Chen et al. 2010; Kuo et al. 2010; Chien and Kuo 2011; Wu et al. 2011; Hendricks et al. 2011). Rain rates derived from the polar-orbiting Tropical Rainfall Measuring Mission (TRMM) satellite observations on 6 and 8 August are shown in Fig. 5. Reflectivity composites of vertical maximum-echo indicator (VMI) from the operational radars in Taiwan are shown in Fig. 6 at intervals of 6 or 12 h during 6–9 August. Whereas most of the deep convection was concentrated in the southern and eastern quadrants of Morakot, the regions northwest of the center were mostly clear. Two persistent rainbands, one nearly east–west oriented across southwestern Taiwan and the other north–south aligned along the windward slopes of southern Central Mountain Range (CMR) on 8 August (Figs. 6e–i), were largely responsible for the extreme rainfall (cf. Fig. 2, also Kuo et al. 2010).

When asymmetric with respect to the center, latent heating (LH) from convection near the core region is known to affect TC motion although its impact is usually

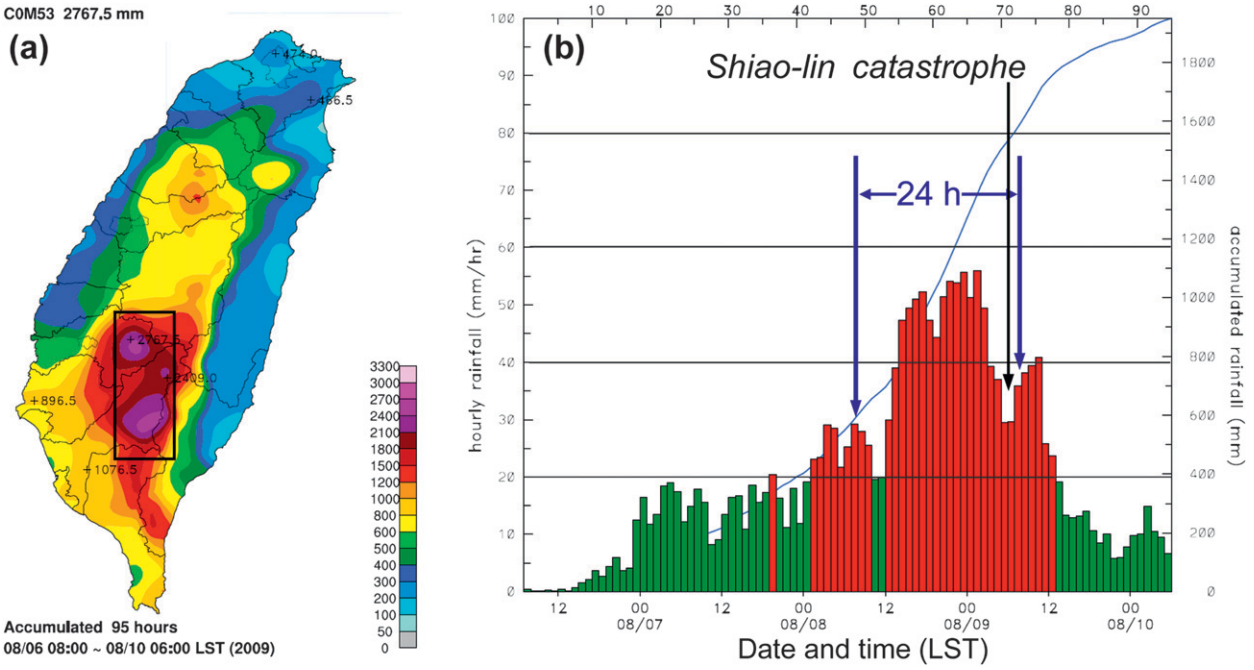

FIG. 2. (a) Total accumulated rainfall (mm; color) over Taiwan and (b) histogram of hourly rainfall (mm h^{-1}; bars, red/green for above/below 20 mm h^{-1}) and accumulated rainfall (mm; blue curve) averaged among all stations inside the box shown in (a) from 0700 LST 6 Aug to 0600 LST 10 Aug 2009 (95 h, from 2300 UTC 5 Aug to 2200 UTC 9 Aug 2009); both courtesy of Dr. L. Feng of the Taiwan Typhoon and Flood Research Institute (TTFRI). The 24-h period of heaviest rainfall on 8 Aug (in UTC) and the time of Shiao-lin catastrophe are indicated in (b).

less significant than those of advection processes (e.g., Willoughby 1992; Wang and Holland 1996). The convective heating can modify potential vorticity [(PV) or relative vorticity] tendency and thus influence TC motion through the advection of symmetric PV by heating-induced asymmetric flow and by direct generation of PV tendency by asymmetric heating, which shifts the TC toward the region of maximum LH (e.g., Chan 1984; Fiorino and Elsberry 1989; Wang and Holland 1996; Wu and Wang 2001; Chan et al. 2002). The effects of asymmetric LH on TC movement have previously been simulated by Wu and Wang (2001) for idealized cases and further estimated by Chan et al. (2002) for real cases using satellite cloud images and prescribed vertical heating profiles. While Chan et al. (2002) propose that the effects of asymmetric LH can be more important in slow-moving TCs, such impacts and their details in real TC cases have yet to be clearly demonstrated.

The overall rainfall distribution associated with a TC in Taiwan has traditionally been viewed as controlled mainly by the TC track, as topographic uplift plays an essential role in rainfall production (e.g., Chang et al. 1993; Wu and Kuo 1999). In the case of Morakot, the persistent asymmetric rainfall pattern (Figs. 4–6) combined with the turning of the storm toward the north-northwest led to the heaviest rain to its rear on 8 August, when the TC was over the northern Taiwan Strait and moved the slowest (cf. Figs. 1–3).

The question addressed in this study is whether Morakot's movement was also, in turn, affected by the rainfall and associated LH during this period besides a weakened steering flow; that is, did a significant interaction occur between the track and asymmetric rainfall such that the LH feedback caused the TC to further slow down upon leaving Taiwan? Thus, the hypothesis is that an additional motion vector (toward the south-southeast/southeast) is produced by the asymmetric and persistent heating (which may be locally enhanced by the high terrain of CMR) and opposes the steering flow (toward the north-northwest) as Morakot was leaving Taiwan, as illustrated in Fig. 7. Thus, the combined motion vector would lead to a slower speed toward the north-northwest on 8 August, and thus lengthening the period of heavy rainfall. In this study, numerical simulations of Morakot will be used to test our hypothesis through a series of sensitivity experiments.

In section 2, the dataset, numerical model, and methodology used in this study are described. The model simulation over the 4-day period when Morakot affected Taiwan are presented and validated, and the sensitivity tests on the effect of LH for a 2-day period upon Morakot's departure are described and discussed in section 3. Further discussion of the model results on the LH effects and additional tests, steering flow analysis, and diagnosis on TC motion are presented in section 4. Finally, the conclusions are given in section 5.

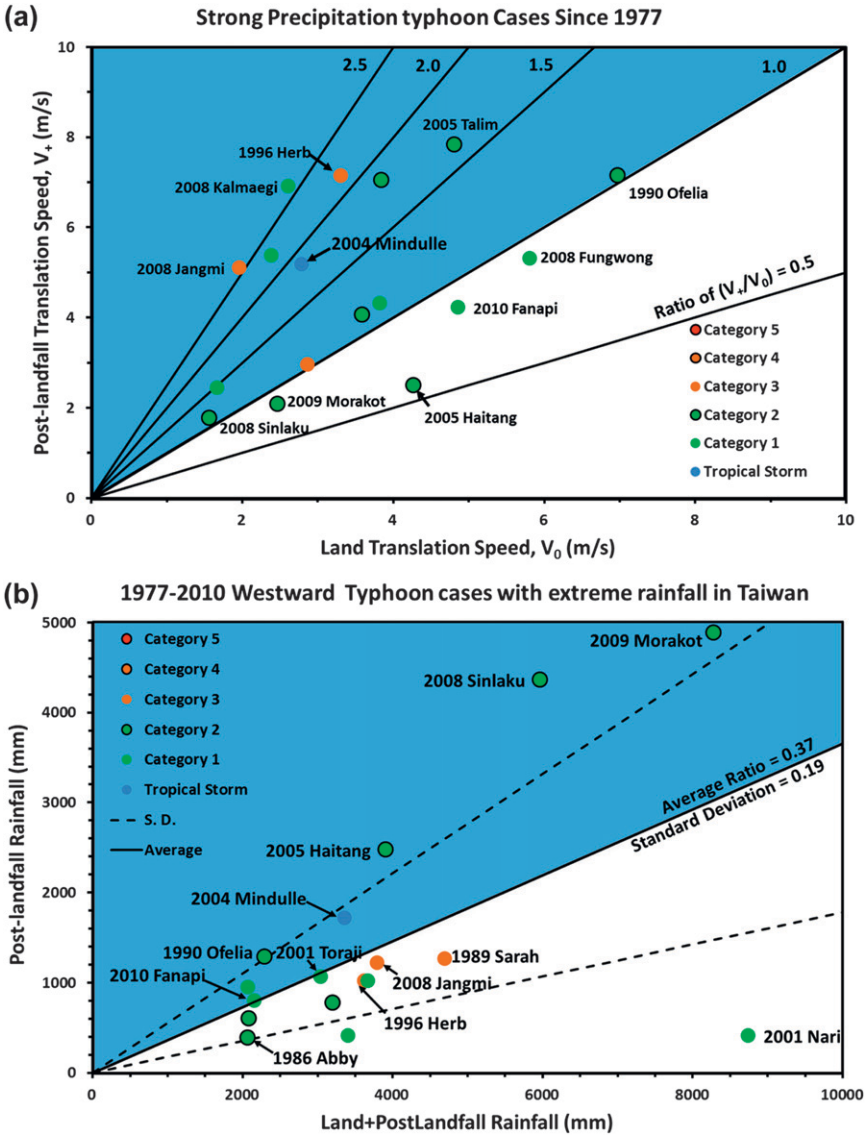

FIG. 3. Scatterplots of (a) translation speed (m s^{-1}) and (b) total rainfall amount (mm) after landfall vs during landfall periods from 18 strong-precipitation (≥2000 mm during and after landfall) typhoons in Taiwan since 1977. The total rainfall is summed over 25 CWB surface stations. The landfall (postlandfall) period is defined as the time from entering to exiting Taiwan (from leaving the coast to a distance of 100 km offshore from the coastline). Different colors denote typhoons [or tropical storm (TS)] of different intensity on the Saffir–Simpson scale (with a maximum sustained wind speed of 64–118 km h^{-1} for TS, and 119–153, 154–177, 178–208, 209–251, and ≥252 km h^{-1} for category 1–5 hurricanes, respectively). In (b), solid and dashed lines denote the mean ratio and one standard deviation, respectively.

2. Data and model experiments

a. Data and methodology

The observations used in this study to examine the evolution and structure of Morakot (2009) and to validate model simulations include the following: The track and basic TC information from the CWB and the Joint Typhoon Warning Center (JTWC); visible (VIS) and infrared (IR) cloud imagery and blackbody brightness temperature T_{BB} data (every 1 h) from the geostationary *Multifunctional Transport Satellite* (*MTSAT*); rain rates derived from the polar-orbiting TRMM satellites; and radar reflectivity VMI composites (every 1 h). Hourly observations from over 400 gauges of the Automatic Rainfall and Meteorological Telemetry System (ARMTS; Hsu 1998) during 6–10 Aug 2009 are used to

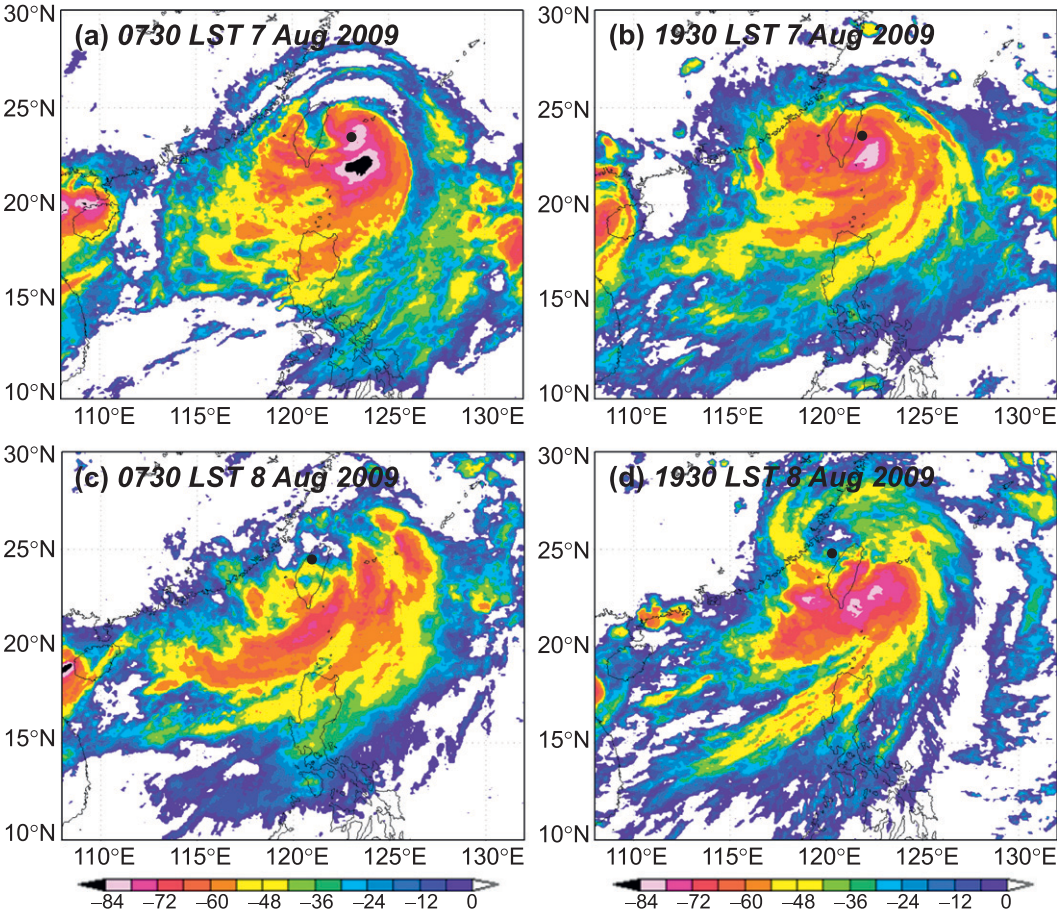

FIG. 4. The Japanese geostationary *MTSAT* IR blackbody brightness (cloud-top) temperature T_{BB} (°C) distributions at (a) 0730 and (b) 1930 LST 7 Aug and at (c) 0730 and (d) 1930 LST 8 Aug 2009. Solid dots denote the center of Morakot. Notice the asymmetric cloud pattern and rainfall around the TC during the period.

validate model rainfall over Taiwan. Several of these datasets have been shown in Figs. 1–7.

To substantiate the model sensitivity tests, steering flow calculations are compared with those by Chien and Kuo (2011) in section 4b using three gridded datasets from two operational centers. In addition to the European Centre for Medium-Range Weather Forecasts (ECMWF) Year of Tropical Convection (YOTC) analyses, the National Centers for Environmental Prediction (NCEP) final analysis at 1° and the ECMWF Tropical Ocean Global Atmosphere (TOGA) advanced analysis at 1.125° latitude/longitude resolutions are examined at 6-h intervals. In section 4c, a simple diagnosis on TC motion is presented from the perspective of TC kinematics in a quasi-Lagrangian framework using the model simulations.

b. Description of the CReSS model

The Cloud-Resolving Storm Simulator (CReSS) model version 2.3 used in this study is a nonhydrostatic, fully compressible, cloud-resolving model developed at the Hydrospheric Atmospheric Research Center of Nagoya University, Japan (Tsuboki and Sakakibara 2002, 2007). This model employs a terrain-following vertical coordinate defined as $\zeta = z_t[z - z_s(x, y)]/[z_t - z_s(x, y)]$, where z_t and z_s are heights at the model top and surface, respectively. Prognostic equations for 3D momentum (u, v, w), pressure p, potential temperature θ, and mixing ratios of water vapor q_v and other hydrometeors q_x (where x denotes a species) are formulated. To properly simulate clouds at high resolution, an explicit bulk cold rain (mixed phase) scheme based on Lin et al. (1983), Cotton et al. (1986), Murakami (1990), Ikawa and Saito (1991), and Murakami et al. (1994) are used without any cumulus parameterization (Table 1). Six species (water vapor, cloud water, cloud ice, rain, snow, and graupel) with microphysical processes of nucleation (condensation), sublimation, evaporation, deposition, freezing, melting, falling, conversion, collection, aggregation, and

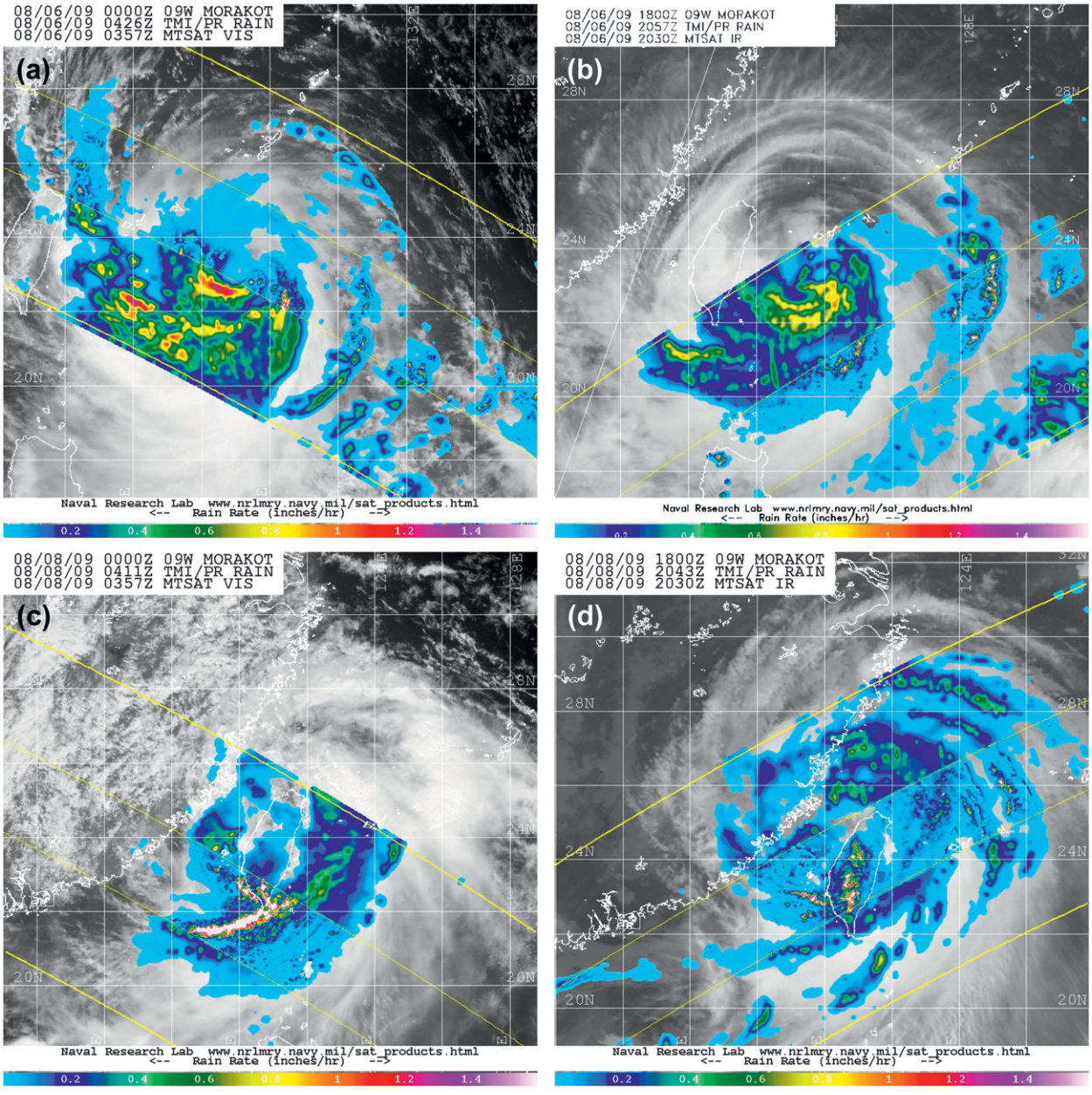

FIG. 5. TRMM precipitation radar (PR) rain rates (in. h^{-1}; color, scale at bottom) overlaid on *MTSAT* VIS (when available) or IR cloud imagery of Typhoon Morakot at (a) 0426 UTC 6 Aug, (b) 2057 UTC 6 Aug, (c) 0411 UTC 8 Aug, and (d) 2043 UTC 8 Aug 2009. The time closest to TRMM PR data and type of *MTSAT* cloud imagery are labeled at the top-left corner of each panel (all panels from the Naval Research Laboratory).

liquid shedding are included (Tsuboki and Sakakibara 2002). Subgrid-scale turbulent mixing is parameterized using 1.5-order closure with turbulent kinetic energy (TKE) prediction (Tsuboki and Sakakibara 2007), and planetary boundary layer (PBL) processes are parameterized following Mellor and Yamada (1974) and Segami et al. (1989). Momentum and energy fluxes and radiation at the surface are also considered with a substrate model (Kondo 1976; Louis et al. 1981; Segami et al. 1989), but the effect of cloud on longwave radiation is neglected.

In the CReSS model, the Arakawa-C staggered and Lorenz grids are used in the horizontal and vertical with no nesting (or domain movement). A time-splitting scheme (Klemp and Wilhelmson 1978) is adopted to integrate fast and slow modes separately for computational efficiency, with the filtered leapfrog method (Asselin 1972) and the implicit Crank–Nicolson scheme for the integration at

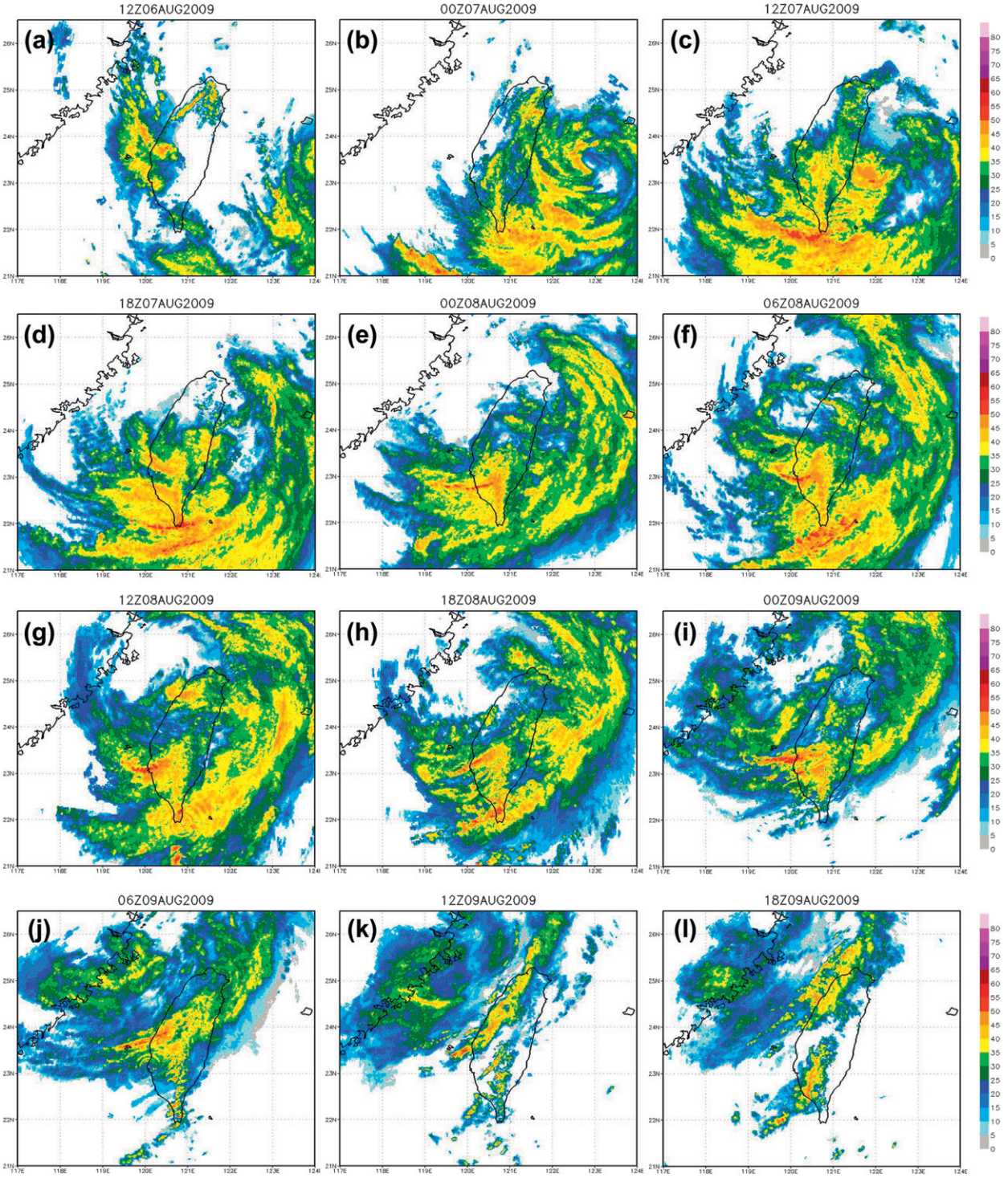

FIG. 6. Radar VMI reflectivity composites (dBZ) in the Taiwan region at (a) 1200 UTC 6 Aug, (b) 0000 UTC 7 Aug, and every 6 h from (c) 1200 UTC 7 Aug to (l) 1800 UTC 9 Aug 2009. Scales are shown on the right.

large (Δt) and small time steps ($\Delta\tau$), respectively (Table 1). The CReSS model has been used to study various types of convective systems and TCs (e.g., Wang and Huang 2009; Wang et al. 2011; Akter and Tsuboki 2012).

c. *Experiment design and sensitivity test*

A total of 19 CReSS model experiments (Table 1) have been carried out with the same grid size of 3 km

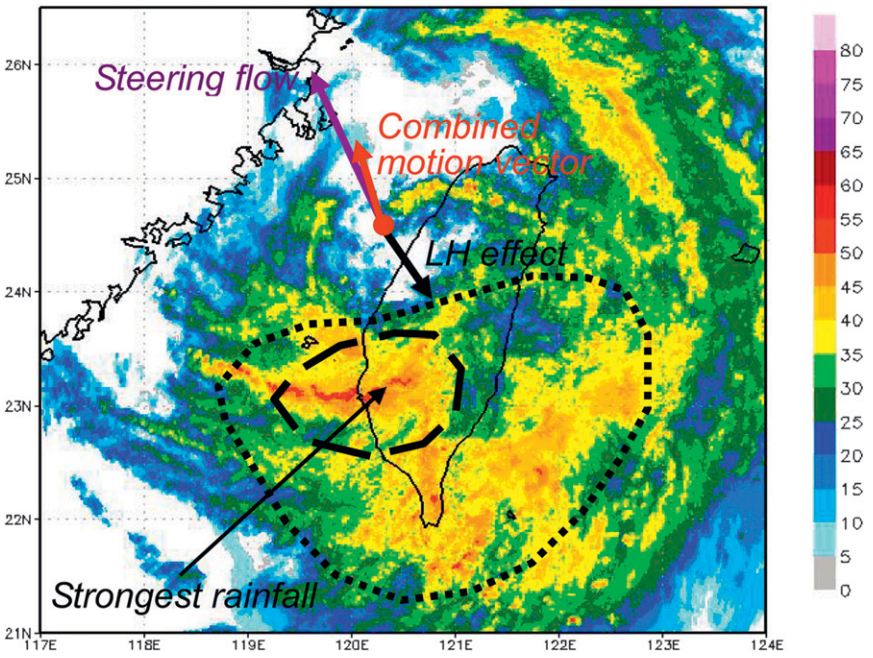

FIG. 7. Schematic of the hypothesis of this study, in which the arrows represent TC motion vectors induced by the steering flow and other effects (purple, toward the north-northwest), by the latent heating (LH; black, toward the south-southeast), and the combined effect (red, toward the north-northwest at a reduced speed). The red dot near 24.5°N, 120.5°E marks the TC center of Morakot upon leaving Taiwan, and the thick dotted and dashed lines enclose the area of asymmetric rainfall, mostly to the south and east of the TC center, from the radar VMI composite at 0800 UTC 8 Aug 2009.

and 50 vertically stretched layers with the model top at 25 km (the minimum Δz at the bottom is 100 m). For 13 runs, the ECMWF YOTC project's (e.g., Waliser and Moncrieff 2007; Moncrieff 2010) 6-h analyses at a resolution of 0.25° latitude/longitude at 20 pressure levels are used as the initial and boundary conditions (ICs/BCs). The first experiment, which is a 4-day control run (CTL1, domain 1 in Fig. 1) starting from 0000 UTC 6 August 2009 with a horizontal grid of 576 × 480 points, closely reproduces the evolution and structural characteristics of Morakot over the period when it affected Taiwan. Therefore, it is considered that the BCs from the ECMWF YOTC gridded analyses have well resolved both the large-scale environment and the outflow of Morakot. At the lower boundary, terrain heights at about 900-m horizontal resolution and weekly sea surface temperature (SST) at 1° × 1° resolution (Reynolds et al. 2002) are provided. For all the runs, outputs were produced every 30 min (Table 1).

A series of 12 runs is then carried out with a domain of 480 × 480 grid points for 2 days starting from 0000 UTC 8 August 2009, which includes the second control run (CTL2, domain 2 in Fig. 1). Two effects are tested through CTL2 and the other 11 sensitivity tests (Table 2): latent heating and Taiwan topography. The effect of LH is examined by altering the water vapor in the ICs/BCs to 100%, 50%, 25%, and 0% of the original values. The Taiwan terrain is changed to 100%, 50%, or 0% of the real height (fixed at 10 m for the last case). The 12 combinations are labeled as R01–R12 (Table 2), with R01 being the control (CTL2). Whereas the moisture content is directly linked to the LH effect associated with a TC, some other factors, such as convergence and instability, may also contribute. The sensitivity tests with reduced vapor amounts can be viewed as if the TC occurred in a drier environment, while those with no initial moisture are quite similar to dry or fake-dry runs commonly used (e.g., Gall 1976; Mullen and Baumhefner 1988; Kuo et al. 1996).

To further confirm the robustness of our sensitivity test results, another six runs are conducted using the NCEP final analysis at 1° × 1° resolution (at 26 levels) and the Japan Meteorological Agency (JMA) regional analyses at a resolution of 0.25° longitude × 0.2° latitude (at 21 levels, both every 6 h) as ICs/BCs, with otherwise identical strategy and configuration to R01–R03 (starting from 0000 UTC 8 August for 48 h). These additional tests are named as N01–N03 (using NCEP data) and J01–J03 (using JMA data).

TABLE 1. Summary of CReSS model configuration of domain and basic setup, physics, and numerical methods used in CTL1 and CTL2. Time integration schemes can be classified as horizontal explicit (HE), vertical explicit (VE), and vertical implicit (VI). An asterisk means that the vertical grid spacing Δz of CReSS is stretched (smallest at the bottom), and the averaged spacing is given in the parentheses.

Domain and basic setup	CTL1	CTL2
Projection	Lambert conformal, center at 120°E, secant at 10° and 40°N	
Grid size (x, y, z)	3 km × 3 km × 100–745 m (500 m)*	
Grid dimension (x, y, z)	576 × 480 × 50	480 × 480 × 50
Domain size (x, y, z)	1728 km × 1440 km × 25 km	1440 km × 1440 km × 25 km
Topography and SST	Real at (1/120)°, and weekly mean at 1° resolution	
ICs/BCs	ECMWF YOTC analyses (0.25° × 0.25°, 20 levels, 6 h)	
Initial time	0000 UTC 6 Aug 2009	0000 UTC 8 Aug 2009
Integration length	96 h (4 days)	48 h (2 days)
Output frequency	30 min	30 min
Model physics		
Advection and diffusion	Both fourth-order in horizontal and vertical	
Cloud microphysics	Bulk cold rain scheme (mixed phase with six species)	
Cumulus parameterization	None	
PBL parameterization	1.5-order closure with TKE prediction	
Surface processes	Energy and momentum fluxes, shortwave and longwave radiation	
Soil model	41 levels, every 5 cm to 2 m deep	
Numerical methods		
Time steps	$\Delta t = 5$ s, $\Delta\tau = 2.5$ s	
Integration method	Filtered leapfrog for Δt (HE-VE), leapfrog and Crank–Nicolson for $\Delta\tau$ (HE-VI)	

3. Model results

a. 4-day control run (CTL1)

The capability of the CReSS model to realistically simulate the entire event of TY Morakot will be first verified using the various datasets listed in section 2a. Tracks from JTWC, from the ECMWF YOTC analysis, and from the CReSS model simulation in CTL1 (from 0000 UTC 6 August to 0000 UTC 10 August) are compared in Fig. 8. The TC locations at each time in the model simulations are manually determined using both the pressure and wind fields near 1.4 km (level 7) over ocean/low terrain or at 3.2 km (level 12) while crossing the CMR. For analysis data, low-level (850–700 hPa) centers are used. Both the JTWC and ECMWF YOTC tracks indicate the slow moving speed (about 5 km h^{-1}) of Morakot upon leaving Taiwan on 8 August 2009. However, larger differences exist during Morakot's passage across Taiwan and at 0000 UTC 8 August when the YOTC analysis has the position at a lower latitude (Fig. 8). Perhaps because the CTL1 experiment employs the ECMWF YOTC analysis as ICs/BCs (section 2c and Table 1), the simulated TC track follows that of YOTC closely. Nonetheless, the tracks in CTL1 and JTWC never differ by more than 120 km during the entire 4-day period, even during Morakot's landfall in Taiwan. It is important that the model reproduces the slow translation speed of Morakot on 8 August 2009 for the correct simulations of rainfall maxima and distribution (to be shown shortly). Furthermore, the sensitivity tests to be discussed in sections 3c and 3d would not be as meaningful if the model had not been able to realistically simulate the evolution of TY Morakot, and particularly its slow moving speed near Taiwan.

The central mean sea level pressure (MSLP) and maximum surface wind simulated in CTL1 are also compared with the observations in Fig. 9. The JTWC has estimated a more intense TC than in the ECMWF YOTC analysis before landfall in Taiwan (6–7 August), but a weaker intensity after about 1800 UTC 7 August due to a rapid intensity drop during landfall (Fig. 9; cf. Figs. 1, 8). In contrast, the TC only weakens slowly in the

TABLE 2. Sensitivity test experiments and their labels for different combinations of reduced water vapor amounts (in ICs/BCs) and reduced terrain heights of Taiwan. The top-left experiment (R01) is the control test (CTL2). The same model setup is used for all tests, which start from 0000 UTC 8 Aug 2009 for 48 h (right half in Table 1). For tests with 0% topography, a flat terrain over Taiwan of 10 m is used.

	Water vapor amount			
Terrain height	100%	50%	25%	0%
100%	R01	R02	R03	R04
50%	R05	R06	R07	R08
0% (10 m)	R09	R10	R11	R12

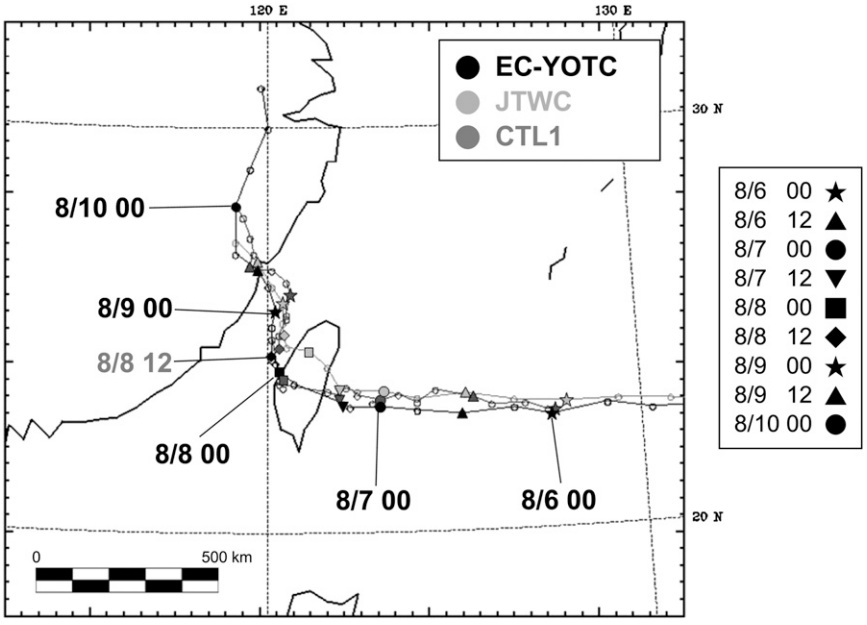

FIG. 8. The predicted track each 3 h for the CTL1 experiment from 0000 UTC 6 Aug 2009 (for 4 days) of the CReSS model simulation, compared with the 6-h JTWC positions and 6-h positions derived from the ECMWF YOTC analyses that are labeled at 0000 UTC each day, with a key position indicated at 1200 UTC 8 Aug. Different symbols (see box on right side) are plotted each 12 h for ease of comparison.

ECMWF YOTC analysis near and after landfall. As might be expected due to the 3-km resolution, the CReSS simulation CTL1 produces a stronger TC by about 7–10 hPa and 14–25 km h^{-1} (~4–7 m s^{-1}) than in the YOTC analysis on 8 August, although the intensity trends are similar. As a result, the TC strength in CTL1 is close to the JTWC estimate prior to landfall but remains stronger near 8 August (Fig. 9). The local speed up due to high resolution with complex terrain (e.g., Miller and Davenport 1998) may have also contributed to the stronger surface winds in the model compared to the JTWC. Notice that the TC intensity trend in CTL2 from 0000 UTC 8 August is also similar to that in CTL1. Overall, the model simulations of TC intensity are considered to be reasonable.

The model-simulated horizontal winds and pressure at about 1.4 km and rain rates from CTL1 at 2100 UTC 6 August (Fig. 10a) and 0200 UTC 8 August (Fig. 10b) can be compared directly with the TRMM rain rates in Figs. 5b,c. On 6 August when Morakot was still about 150 km east of Taiwan, the asymmetric rainfall and rainband structure are both well captured. On 8 August when Morakot had moved offshore from Taiwan (Fig. 10b is about 2 h earlier than Fig. 5c), the model is able to simulate key features of the asymmetric structure, including the intense rainband near the southern tip of Taiwan and three relatively dry regions near the TC center, and northern and eastern Taiwan (cf. Figs. 6f, 8). The CTL1 model-simulated column maximum mixing ratio of total precipitating hydrometeors (rain, snow, plus graupel) every 12 h from 1200 UTC 6 August to 1200 UTC 9 August 2009 (except every 6 h on 8 August) is shown in Fig. 11, which can be compared with the radar VMI reflectivity composites in Fig. 6. Comparison of these two figures confirms that the model reproduces the persistent asymmetric rainfall structure associated with Morakot throughout this period, as well as the general location of rainbands and heavy rainfall over and surrounding Taiwan.

The total (Fig. 2a) and daily rainfall distributions (Figs. 12b–d) over Taiwan observed by the rain gauge network (Fig. 12a) are used to validate the 4-day CTL1 model run (Figs. 12e–h). With nearly identical accumulation periods, the model-simulated total rainfall in CTL1 (Fig. 12e) agrees very well with the observations (Fig. 2a) in both pattern and amount, including a peak value slightly over 3000 mm over the southern CMR. The 24-h daily accumulated rainfall from 7 to 9 August (in LST) in the model (Figs. 12f–h) also compares favorably with the observations (Figs. 12b–d). Notice the local maxima over the mountains in northern (near 24.5°N) and central Taiwan (near 23.5°N) on 7 August (Figs. 12b,f), the large rainfall amounts over the southern plain areas west of CMR (although somewhat underpredicted) on 8 August (Figs. 12c,g), and the

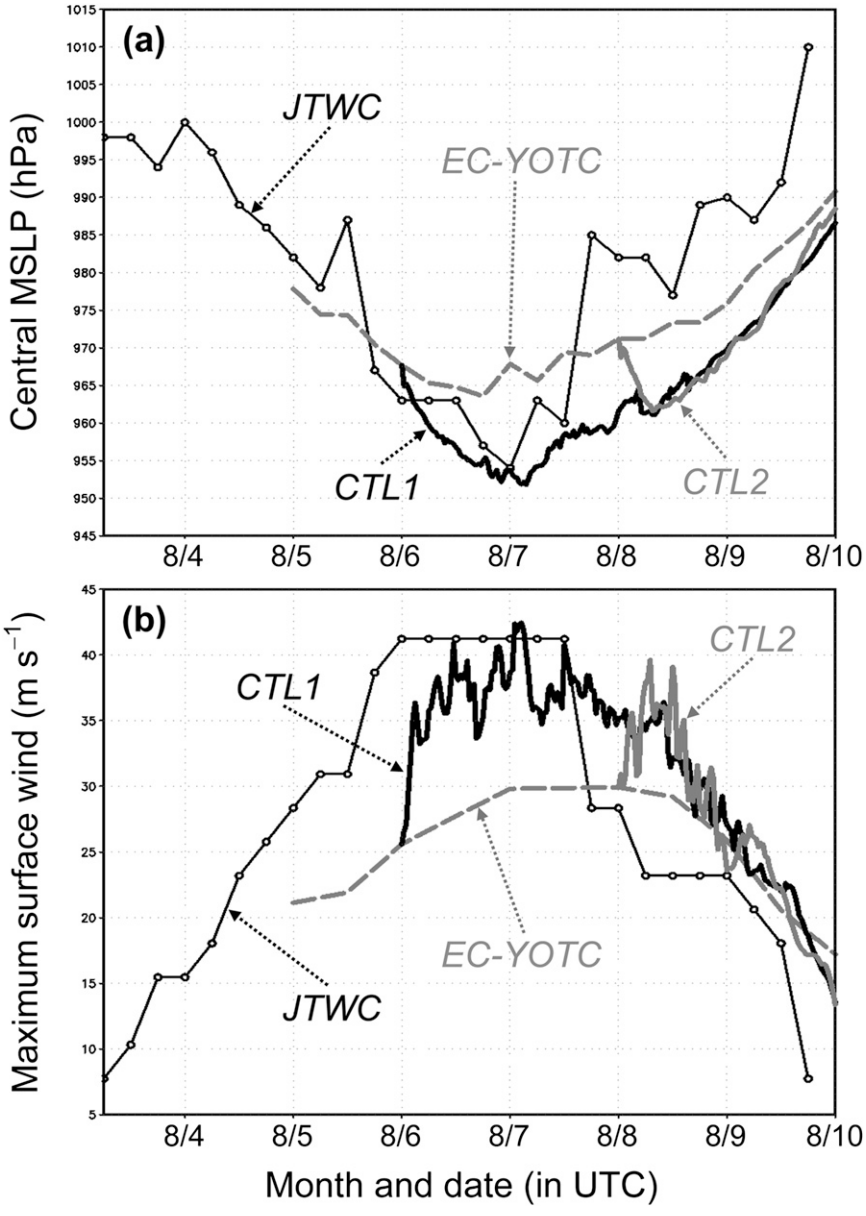

FIG. 9. Comparison of CTL1 (thick black, from 0000 UTC 6 Aug) and CTL2 (thick gray, from 0000 UTC 8 Aug) simulated (a) central MSLP (hPa) and (b) maximum surface (10-m) wind speed (m s^{-1}) with values from the JTWC best track (solid line with open circles) and from the ECMWF YOTC analyses (gray dashed, from 5 Aug).

details between the maxima over central and southern Taiwan on 9 August (Figs. 12d,h). However, the model seems to overpredict the rain along the ridge of the southern CMR at 22.3°–22.8°N. Other mesoscale models, including the Weather Research and Forecasting Model (WRF), also have this tendency for the Morakot case (e.g., Nguyen and Chen 2011, their Figs. 12 and 18; Fang et al. 2011, their Figs. 1 and 4). It is noted that few rain gauges exist in this remote region of the southern CMR (Fig. 12a), so the model tendency to overforecast rainfall here remains uncertain and requires further study.

The hourly rainfall simulated in CTL1 (Fig. 13a) averaged over the rectangular region in Fig. 2a may be compared with the observed evolution in Fig. 2b. For this region of heaviest rainfall, the CReSS model reproduces the rainfall evolution quite well, especially during the heaviest rain over 0600–1800 UTC 8 August, when Marokot was leaving Taiwan (Figs. 2b, 13a, and cf. Figs. 1, 8). As discussed earlier, such a realistic rainfall

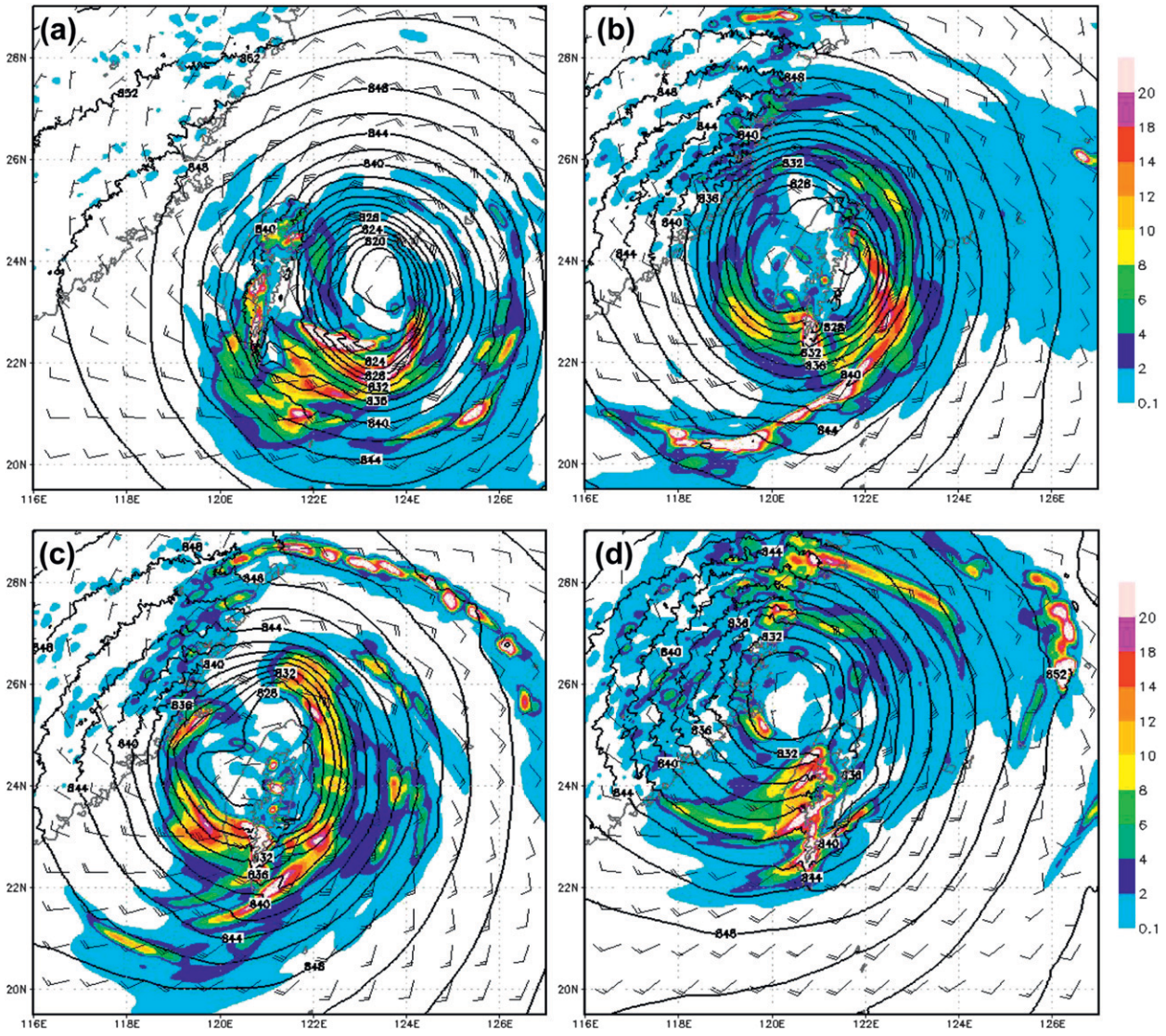

FIG. 10. Model-simulated rain rates (mm h^{-1}; color, scale on right), and pressure (hPa; contours) and wind barbs (full barb = 10 m s^{-1}) at z = 1397 m from CTL1 at (a) 2100 UTC 6 Aug and (b) 0200 UTC 8 Aug, and from CTL2 at (c) 0430 UTC and (d) 2130 UTC 8 Aug 2009.

evolution over the CMR would not be possible without a successful simulation of storm track.

b. 2-day control run (CTL2)

Because the hypothesis in this study is that the latent heating associated with the heavy rainfall during 8 August when Morakot was over the Taiwan Strait contributed to its slow motion, the sensitivity tests are performed only for 2 days from 0000 UTC 8 August 2009 (Table 1). In all of these tests, the TC starts from the same location with the identical initial vortex structure and experiences nearly the same ambient flow at least during the early stages of the simulation, which is the period of greatest concern.

As listed in Table 1 (right half), the domain of CTL2 control run, with grid dimensions of 480 × 480 × 50, is centered on Morakot as it entered the Taiwan Strait (cf. Figs. 1, 8). Recall that the trends in central MSLP and maximum wind in CTL2 are very similar to those in CTL1 (Fig. 9). Thus, although close to that in the YOTC analysis, the predicted TC intensity in CTL2 is also stronger than in JTWC for similar reasons as discussed earlier. The simulated rain rates in CTL2 at 0430 and 2130 UTC 8 August (Figs. 10c,d) compare well with the TRMM observations (Figs. 5c,d), in that the model is able to reproduce the asymmetric rainfall pattern and rainband structure, including the general locations of the outer rainbands (also cf. Figs. 6f,h,i). Likewise, the

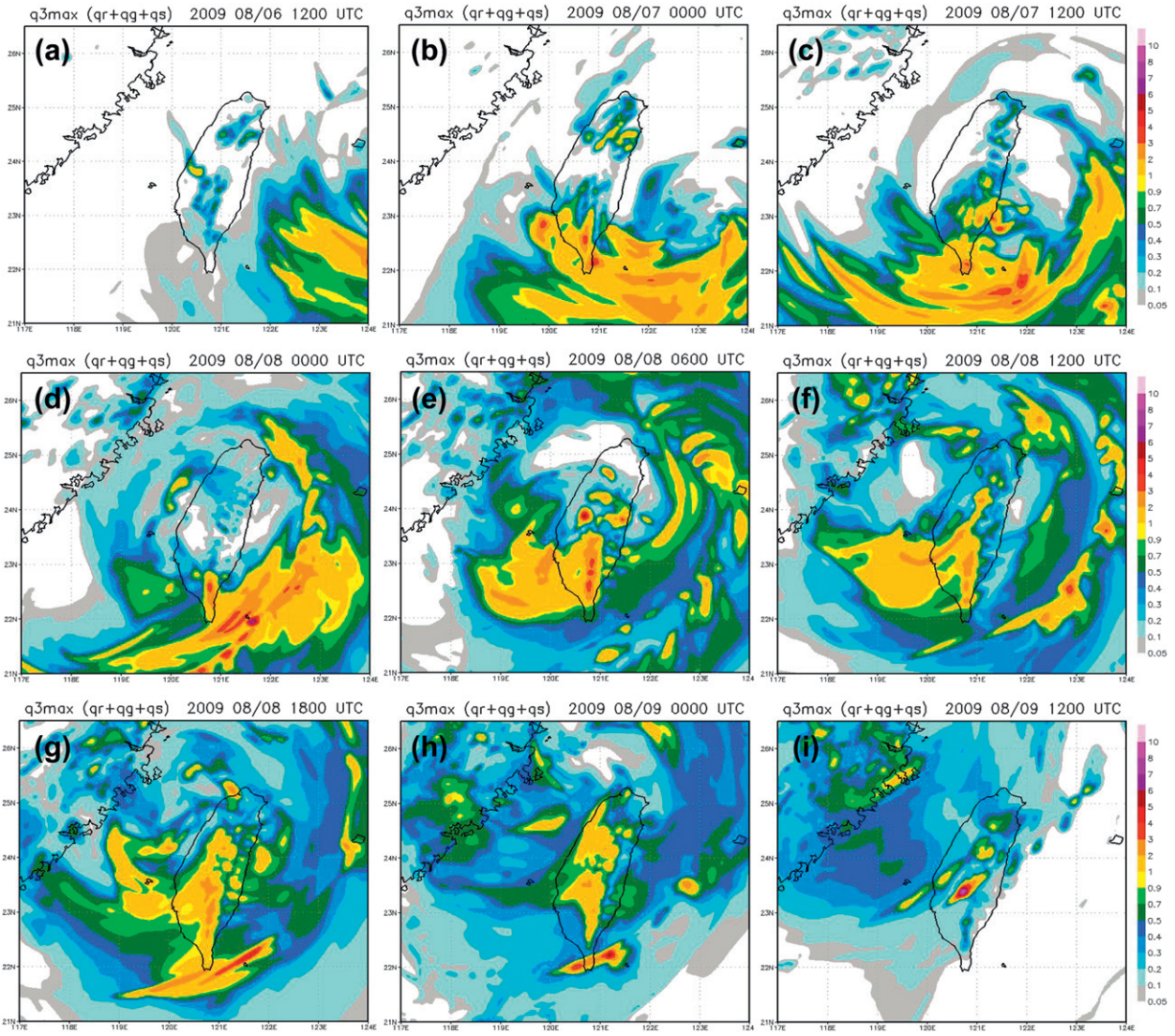

FIG. 11. Model-simulated column maximum mixing ratio of total precipitating hydrometeors (g kg^{-1}, rain + snow + graupel) in CTL1 every 12 h from (a) 1200 UTC 6 Aug to (c) 1200 UTC 7 Aug, every 6 h from (d) 0000 UTC 8 Aug to (h) 0000 UTC 9 Aug, and at (i) 1200 UTC 9 Aug 2009. Scales are shown on the right.

CTL2-simulated column maximum mixing ratios of total precipitating hydrometeors at selected times during 8–9 August 2009 (Fig. 14) also compare quite favorably with the radar VMI reflectivity composites (Figs. 6e–i,k). Notice especially the rainbands parallel over windward slopes and roughly perpendicular to the southern CMR on 8 August, which are essential to the prediction of maximum rainfall.

The CTL2-simulated total and daily rainfall distributions (Figs. 12j–l) and hourly rainfall evolution averaged over the rectangular area in the southern CMR (Fig. 13b) are also compared with the observations (Figs. 12c,d,i, 2b). Although the precipitation in CTL2 is slightly larger than in CTL1 on 8 August (Figs. 13a,b and also Figs. 11d–g, 14), the overall evolution of TY Morakot is considered to be well simulated in CTL2 (Figs. 9, 10c,d, 12j–l, 13b, 14).

c. Sensitivity tests on effects of moisture content

The TC tracks (near 1.4 km) for the sensitivity tests R01–R12 (where R01 is CTL2, cf. Table 2) are plotted in Figs. 15a–c. The focus here is whether discernible and consistent differences in the tracks are predicted when atmospheric moisture (and thus the LH effect) or the terrain heights are gradually reduced. For the four experiments using 100% terrain but different initial water vapor amounts (R01–R04, Fig. 15a), the TCs in the runs with higher moisture content were predicted to move

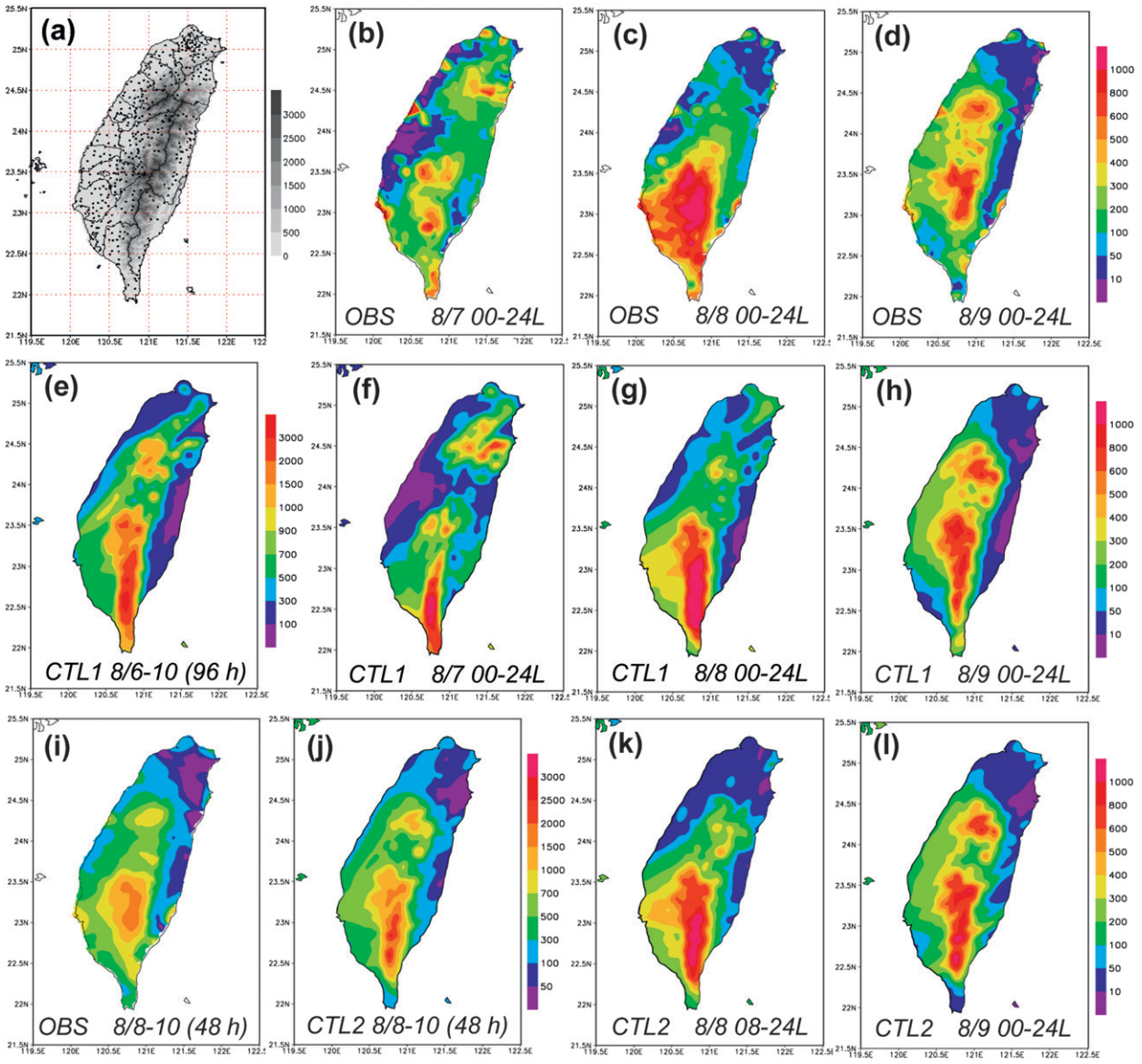

FIG. 12. (a) Terrain heights (m, scale on right) and distribution of rain gauges over Taiwan during the Morakot period. (b)–(d) Observed daily rainfall (mm) for 7–9 Aug (0000–2400 LST), respectively. (e) Model-simulated 4-day total rainfall (mm) during 0000 UTC 6–10 Aug in CTL1. (f)–(h) As in (b)–(d), but from CTL1 model simulation. (i) Observed and (j) model-simulated 48-h rainfall (mm) in CTL2 during 0000 UTC 8–10 Aug, and rainfall (k) during the first 16 h (0800–2400 LST 8 Aug) and (l) during 16–40 h (0000–2400 LST 9 Aug) in CTL2. Scales are plotted to the right of each group with the same accumulation length.

more slowly over 0000–1200 UTC 8 August; that is, the TC position in R01 (100%) remains closer than that in R02 (50%), while those in R03 (25%) and R04 (no moisture) are farther from the coastline by 1200 UTC. After some slow looping motion, the R01 storm picks up some speed during the next 12 h, but it is still the closest to Taiwan at 0000 UTC 9 August (Fig. 15a). By contrast, the TCs in R03 and R04 have moved the farthest by 0000 UTC 9 August and made landfall over China. Subsequently, all four storms begin to converge by 1200 UTC 9 August and have roughly the same translation speed through 0000 UTC 10 August (Fig. 15a).

In the R05–R08 sensitivity tests using 50% terrain, a similar slower translation speed in the test with more moisture is again evident during 0000–1200 UTC 8 August. The R08 test with no initial water vapor has moved the farthest and has made landfall in China at 0000 UTC 9 August (Fig. 15b). In the R09–R12 sensitivity tests using 0% terrain, a similar result is predicted with the speed differences most evident during the first 12 h (Fig. 15c).

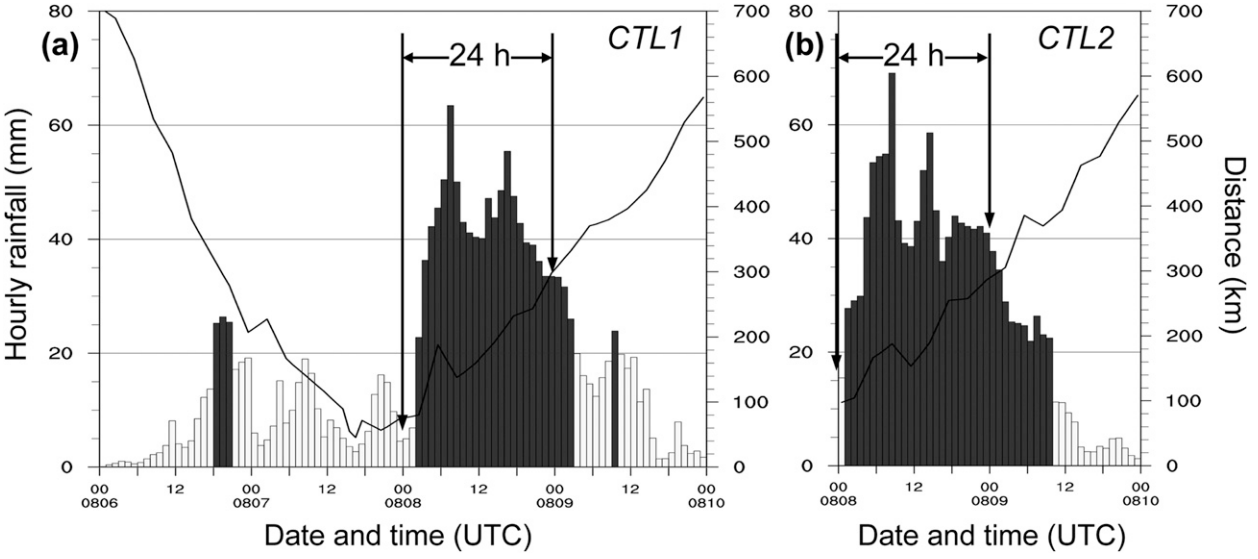

FIG. 13. Histogram of hourly rainfall (mm, bars, gray/white for amounts above/below 20 mm, scale on left) over southern Taiwan (cf. box area in Fig. 2a) and the distance from the TC center to the center of the box (km; curve, scale on right) as simulated by the CReSS model in (a) CTL1 and (b) CTL2. The 24-h period on 8 Aug (in UTC) is marked by a pair of vertical arrows in both panels.

The summary of the track sensitivity to the initial moisture content is that the net motion of all TCs is toward the north-northwest during 8–9 August. The R01, R05, and R09 tests with full moisture content have the slowest motion and move more toward the north. In contrast, the R03, R04, R07, R08, R11, and R12 tests with little or no initial water vapor tend to move more rapidly toward the northwest.

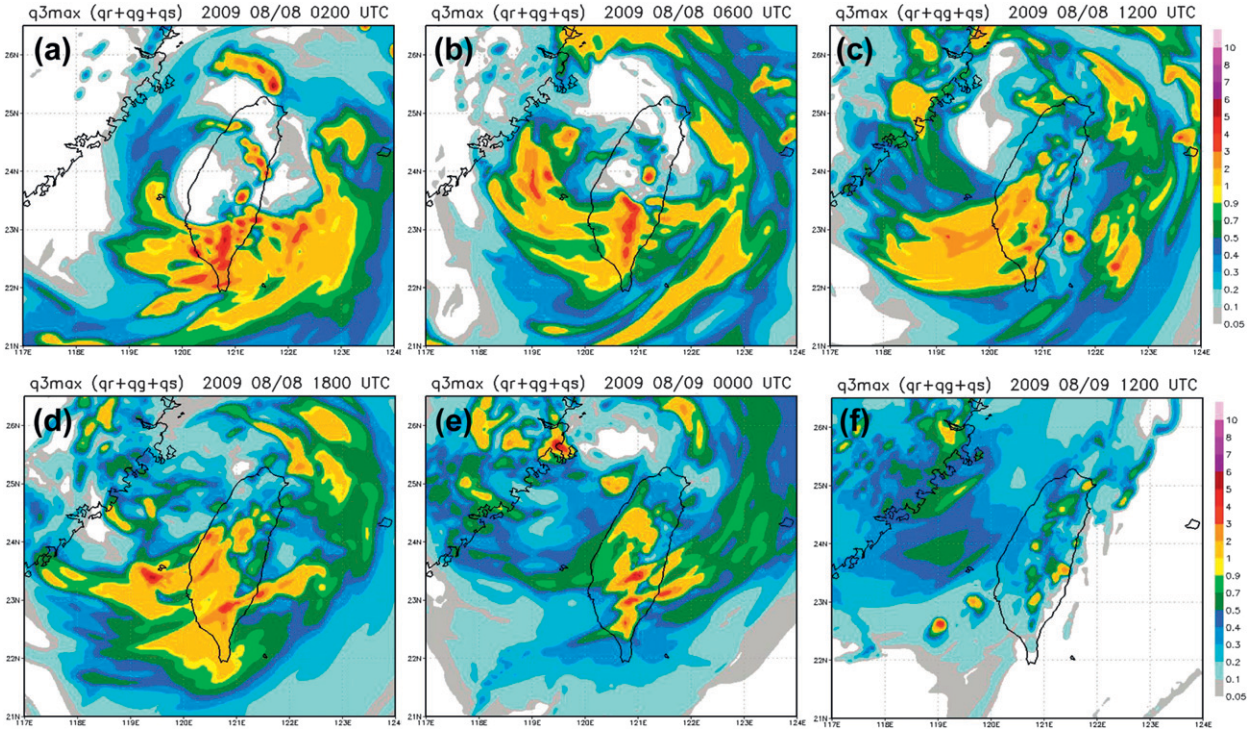

FIG. 14. As in Fig. 11, but from CTL2 at (a) 0200 UTC 8 Aug, and every 6 h from (b) 0600 UTC 8 Aug to (e) 0000 UTC 9 Aug, and at (f) 1200 UTC 9 Aug 2009. Scales are shown on the right.

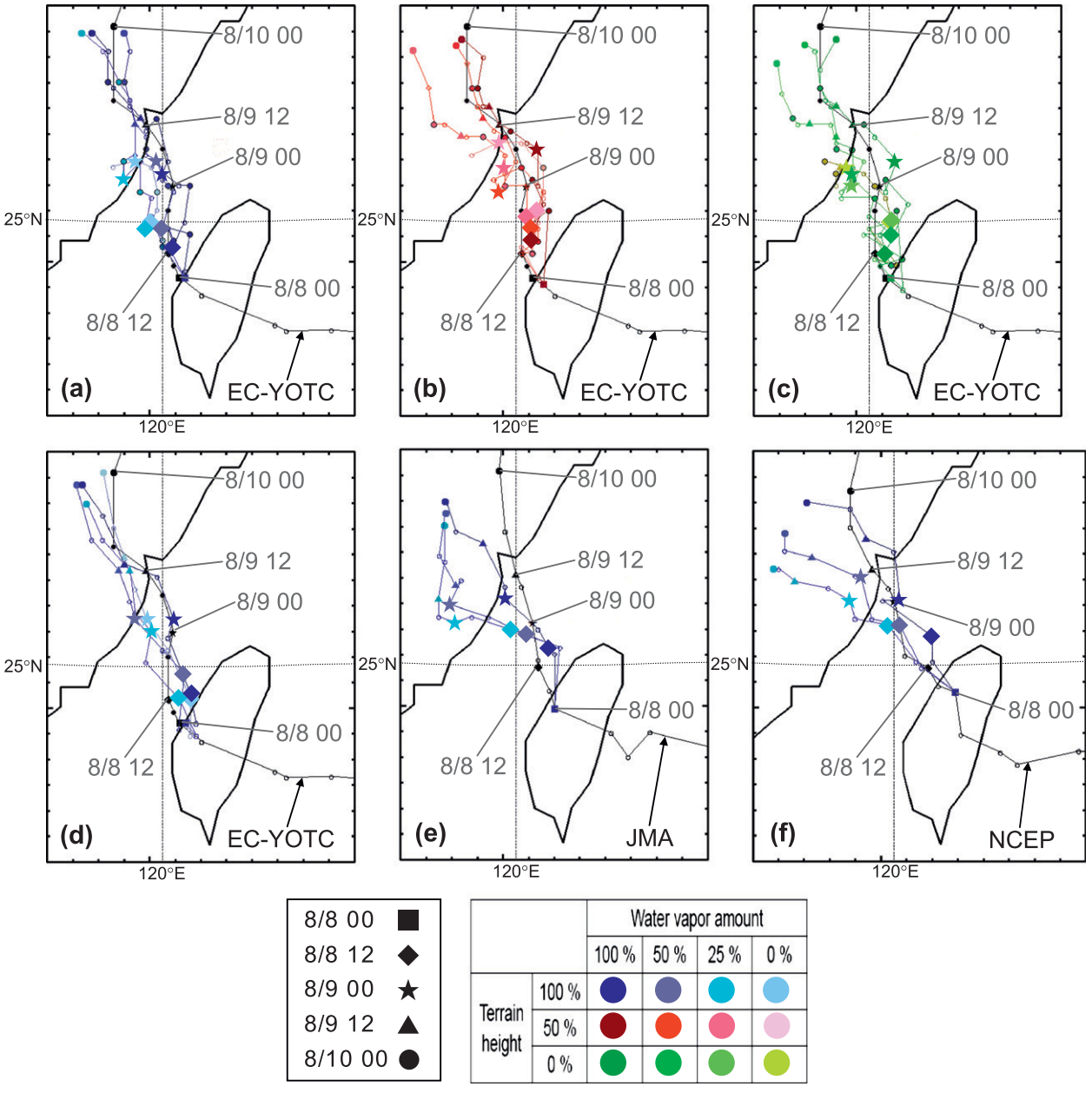

FIG. 15. Model-simulated tracks of Morakot (at low level near 1.4 km) from sensitivity tests (a) R01 (CTL2)–R04, (b) R05–R08, and (c) R09–R12 in which the water vapor amounts and terrain heights are varied (see boxes at bottom) as described in Table 1, with ECMWF YOTC track also plotted. Symbols for 1200 UTC 8 Aug and 0000 UTC 9 Aug are enlarged to highlight these critical times. (d) As in (a), but for upper-level track near 6.1 km from 6-h positions. (e),(f) As in (a), but from tests (e) J01–J03 (every 6 h, with track in JMA analyses plotted) and (f) N01–N03 (with track in NCEP analyses plotted).

The low-level pressure fields at a height near 1.4 km clearly indicate the differences in TC locations among R01 (CTL2), R02, and R03 at 1200 UTC 8 August in Figs. 16a–c, where the 16-h total rainfall distributions over 0000–1600 UTC 8 August are also shown. Thus, the effect of the slower translation speed of the storm in R01 is evident. Azimuthal variations of the average rainfall in 22.5° sectors within the 400-km radius from the TC center for the same period in the sensitivity tests with nonzero initial water vapor are shown in Fig. 17 to illustrate the effect of moisture reduction on rainfall and its asymmetry. In all tests with no initial moisture, such as R04, no rain is predicted, so they are not included. With close agreement with the observations (cf. Figs. 12c,k, 16a), the largest and most narrow rainfall to the south of the TC center is predicted with the largest

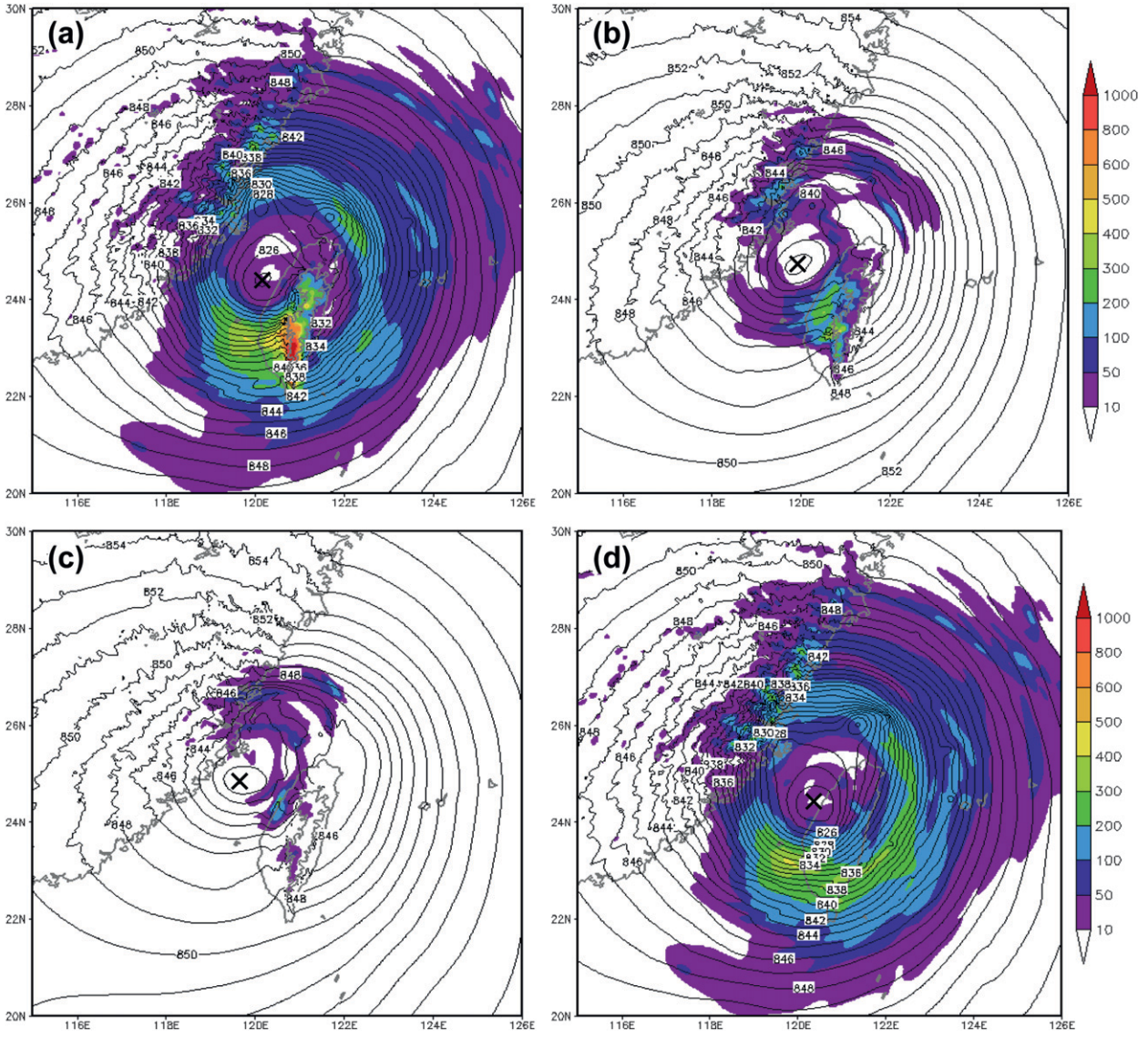

FIG. 16. Model-simulated pressure (hPa; solid contour) at $z = 1397$ m at 1200 UTC 8 Aug and 16-h rainfall (mm) during 0000–1600 UTC 8 Aug 2009 in sensitivity test (a) R01 (CTL2), (b) R02, (c) R03, and (d) R09. In all panels, the 1397-m terrain height contour is also drawn (thick gray) and TC centers are marked by crosses.

asymmetry in R01 (Fig. 17a). Very little asymmetry is predicted for 50% water vapor (R02, cf. Fig. 16b) and almost no asymmetry for 25% water vapor (R03, cf. Fig. 16c). For the 50% terrain tests in Fig. 17b, the 100% water vapor (R05) has a somewhat reduced and broader rainfall distribution to the south, and again greatly reduced rainfall asymmetry for 50% (R06) and 25% water vapor (R07). The no-terrain test (Fig. 17c) has an asymmetry only for the 100% water vapor (R09). It is clear that the rainfall asymmetry (and thus LH) is significantly affected by the moisture content in our tests. Notice also the slowest translation speeds are associated with the 100% water vapor tests (R01, R05, and R09) in Fig. 17. These translation speed differences are summarized in detail in Table 3. Significant reductions in translation speed occur in the first 12 h as the storm is leaving the coast. The reduction in speed becomes much less consistent in the second 12 h, and little effect continues on 9 August. These translation speed reductions with the largest rainfall asymmetries during 0000–1200 UTC 8 August (Fig. 17) are in agreement with the hypothesis illustrated in Fig. 7.

d. Effects of Taiwan topography

The effects of Taiwan topography can also be examined by comparing the tracks in Figs. 15a–c with different terrain heights. For the three sensitivity tests with

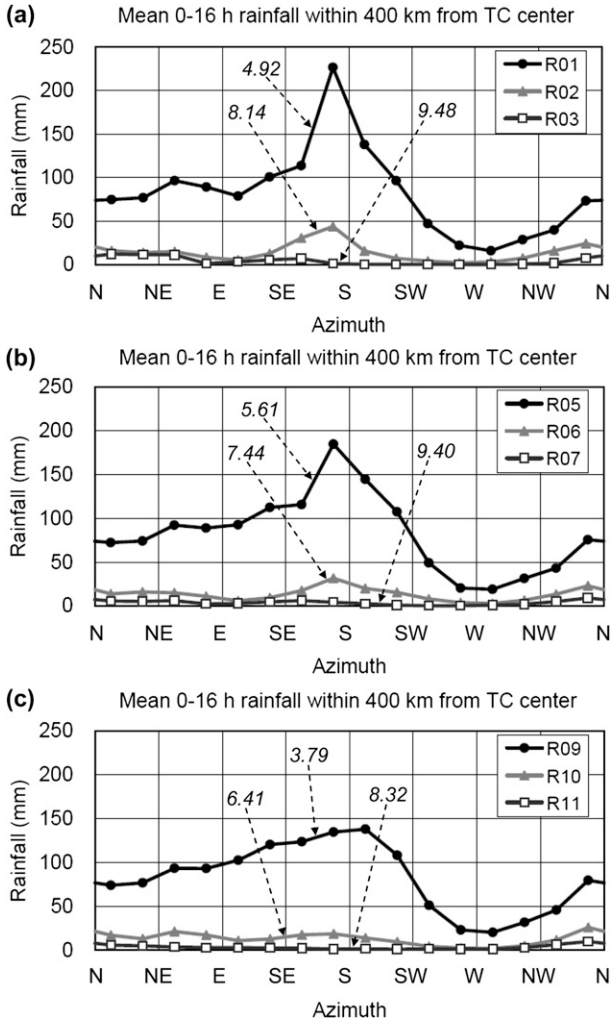

FIG. 17. Total rainfall (mm) during 0000–1600 UTC 8 Aug 2009 averaged in 22.5° azimuthal sectors within a radius of 400 km from the TC center in all sensitivity tests with reduced water vapor, which are labeled (a) R01–R03, (b) R05–R07, and (c) R09–R11 as described in Table 2. The TC translation speed (km h^{-1}) during 0000–1200 UTC 8 Aug in these tests is also marked.

full moisture content (R01, R05, and R08), the model TC locations are all very close at 1200 UTC 8 August. By 0000 UTC 9 August, even though the storm in R01 is the closest to Taiwan (i.e., has moved the slowest on average), the position differences are small. As indicated from the rainfall asymmetries between R01 in Fig. 17a and R05 in Fig. 17b, the peak rainfall in southern Taiwan (to the south-southeast of the TC center) is reduced with a lower topography. It is believed, however, that a large part of this asymmetry is also due to the interaction of monsoon flow and typhoon circulation (e.g., Chien and Kuo 2011; Wu et al. 2011); that is, Morakot was relatively large in size and had an asymmetric rainfall pattern well before it encountered the terrain of Taiwan (cf. Figs. 4–6). In the sensitivity tests with reduced terrain (Figs. 17b,c), the decrease of rainfall over southern Taiwan is somewhat compensated by an increase of rain on the leeside (east-southeast to south-southeast, Fig. 16d). Hence, Taiwan's topography has a relatively smaller impact on the track of Morakot than a reduced water vapor amount, although it has a vital role in the local rainfall production as shown in Figs. 16a,d (also Wu et al. 2002; Ge et al. 2010).

4. Discussion and diagnostics on TC motion

a. Discussion of model results and additional tests

The summary of translation speeds and directions for the sensitivity tests (Table 3) indicates significant speed differences during the first 12 h over 0000–1200 UTC 8 August but not in terms of the moving directions, which are between north-northwest and north (cf. Figs. 15a,c). Consistently, the TCs with 100% water vapor and the largest LH effects (R01, R05, and R09) move at only about 5 km h^{-1}. An increase in translation speed is predicted as the initial moisture content is reduced by half (R02, R06, and R10), and further to about 9–10 km h^{-1} in tests with little or no (0%–25%) moisture (Table 3, left column).

As discussed earlier, the storm in R01 has increased significantly in translation speed during the next 12 h (1200–2400 UTC 8 August), but it remains closer to Taiwan than those in R02–R04 because of its slow motion during 0000–1200 UTC. In general, for 1200–2400 UTC, the storms that still fit the relationship of a faster movement with less rainfall to the south include R03 and R04, R06–R08, and R11 and R12 but not the others (Table 3, middle column), so the results become inconsistent. The reduced sensitivity of the TC track to moisture during the second 12-h period on 8 August is likely due to at least two reasons. First, the strong convection occurs closer to the TC center before 1200 UTC. Wu et al. (2011) indicates that the primary rainfall associated with Morakot expanded outward with time and stayed over southern Taiwan when the TC center moved northward during the postlandfall period. Thus, the sensitivity of the storm track to LH is reduced after 1200 UTC as the model TC center moves farther away from the area of heavy rainfall, also in agreement with Wang and Holland (1996). Second, it is also likely that the slow motion during 0000–1200 UTC 8 August may have augmented the impact of the LH effect as suggested by Chan et al. (2002), since slower-moving rainbands may have generated stronger and more effective local heating. On 9 August, the translation speeds are all around 10–11 km h^{-1} in the same direction regardless of the moisture amount or topography (Table 3, right column) as the TC gradually weakened (cf. Fig. 9).

TABLE 3. Summary of TC translation speeds (1 km h^{-1} = 0.28 m s^{-1}) and directions during two 12-h time periods on 8 Aug and the 24-h period on 9 Aug for the sensitivity tests R01–R12 as described in Table 2. All entries are computed using the locations of TC center at the two endpoints of each period (as in Figs. 15a–c). An entry of ''N/A'' indicates that the low-level TC center had disappeared during the corresponding time period.

	0000–1200 UTC 8 Aug (12 h)		1200–2400 UTC 8 Aug (12 h)		0000–2400 UTC 9 Aug (24 h)	
Expt	Speed (km h^{-1})	Direction (°)	Speed (km h^{-1})	Direction (°)	Speed (km h^{-1})	Direction (°)
R01	4.92	340	11.22	351	11.98	333
R02	8.14	335	10.20	355	10.04	345
R03	9.48	324	8.14	332	11.60	343
R04	9.75	329	9.59	345	N/A	N/A
R05	5.61	351	13.89	4	10.22	324
R06	7.44	353	7.53	317	10.72	342
R07	9.40	350	8.14	335	11.36	321
R08	10.17	360	11.78	330	N/A	N/A
R09	3.79	347	13.97	7	10.36	333
R10	6.47	360	10.99	327	10.43	339
R11	8.32	360	8.13	313	10.99	327
R12	8.32	360	10.74	321	N/A	N/A

When the moisture content is decreased in the model, two effects other than the reduction in asymmetric LH need to be considered. First, the overall reduction of LH (and rainfall, cf. Figs. 16, 17) also leads to a weakening of the vertical coupling mechanism from deep convection, and the upper- and lower-level TC vortices may become decoupled and drift separately (e.g., Wang and Holland 1996; Wu and Wang 2001). Second, the different tracks among the sensitivity tests can result in variations in the mean (steering) flow. The mean ambient flow computed from the 0.25° × 0.25° ECMWF YOTC analyses within a radius of 700 km from the TC center (over a circular area with equal weights) for the period of 0000–1200 UTC 8 August (Fig. 18) indicates a relatively strong southerly flow at low levels (about 5 m s^{-1} near 850 hPa) and a weak northerly flow aloft (<2 m s^{-1} near 300 hPa). The vertical wind shear vector thus pointed toward the south. Notice that the strongest convection was mainly to the downshear left of the TC (cf. Figs. 5c, 6e–g) and consistent with the findings of Corbosiero and Molinari (2002, 2003). The stronger southerly flow at low levels may contribute to a more rapid northward movement of the TC seen in Figs. 15a,c to some extent once it becomes decoupled from the vortex aloft. The TC tracks determined from the upper-level center near 6.1 km (Fig. 15d), nonetheless, again show a faster motion in R02 compared to R01 when the initial moisture content is reduced from 100% to 50% (also Table 4). A similar relative displacement between the upper-level TCs with respect to the low-level centers is also maintained in R01 and R02 (Figs. 15a,d) during 0000–1200 UTC 8 August. In other words, the TC in R02 is still vertically coupled and the low-level storm does not move significantly faster than the upper-level one compared to the vortex in R01, at least up to 1200 UTC 8 August (cf. Table 4). Only when the initial moisture content is further reduced to 25% or less in R03 and R04 does the upper-level vortex start to lag the low-level center (Figs. 15a,d), which is clearly due to the much weaker ambient flow near 400–500 hPa (cf. Fig. 18). These changes in the TC movement indicate some vertical decoupling of the vortex. Since the low-level vortices in R03 and R04 maintain a more consistent behavior and move only slightly faster than the TC in R02 (cf. Fig. 15a), as would be expected from a further reduction of LH asymmetry, the impact of vertical decoupling appears to be stronger at upper levels. Compared to that in R01, the TC in R03 is also accompanied by a slight weakening in the southerly deep-layer mean flow by 2.4 km h^{-1} (0.67 m s^{-1}) during 0000–1200 UTC 8 August (Fig. 18). Although small, this difference can also account for a fraction of the slow motion of the upper-level vortex in R03 (and likely R04 as well).

To further confirm the robustness of our results, six additional tests are performed using gridded data from JMA (the regional analyses) and NCEP (final analyses), as described in section 2c. Named as J01–J03 and N01–N03, respectively, these tests are otherwise identical to R01–R03 (cf. Tables 2, 3) except for the data source of ICs/BCs. Their main results following the same procedure are shown in Figs. 15e,f and Table 5. The tracks are generally more toward the northwest, and both tests using full moisture content (J01 and N01) yield a TC translation speed near 9 km h^{-1} during 0000–1200 UTC 8 August. Although these experiments predict less of the slow motion compared to R01, the reduced moisture tests do consistently show an increasingly faster translation speed during the first 12 h (Figs. 15e,f, Table 5).

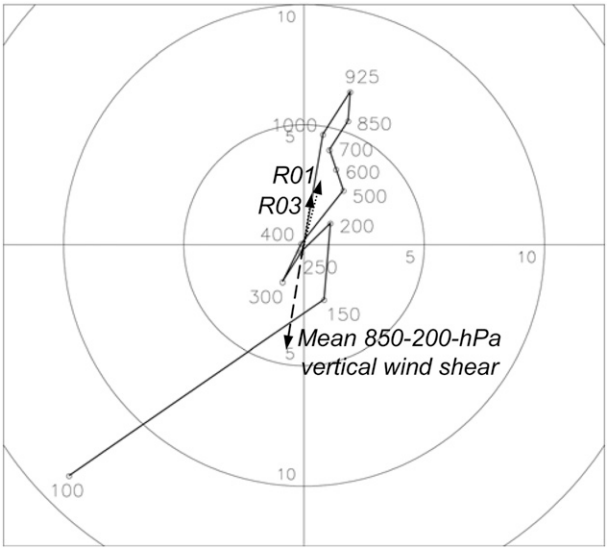

FIG. 18. Hodographs of the mean flow (m s^{-1}) computed from the ECMWF YOTC analyses over a circular area within the radius of 700 km from the TC center during 0000–1200 UTC 8 Aug 2009. Numbers indicate pressure levels (hPa) at nearby dots on the curve. Mean 850–200-hPa vertical wind shear vector (dashed arrow) and deep-layer mean wind vector (averaged over 3–7 km and the same circular area with respect to TC) in R01 and R03 (dotted arrows) are plotted and labeled.

For this period, the speed differences are about 4.5 km h^{-1} between J01 and J03 and 5.4 km h^{-1} between N01 and N03, both comparable to those between R01 and R03 (cf. Table 3). Between the full and 50% moisture tests, where the TC vortices are vertically coherent and intact (not shown), the corresponding speed increase is 2.6 (from J01 to J02) and 4.3 km h^{-1} (from N01 to N02) and a similar behavior also occurs during 1200–2400 UTC 8 August (Table 5). It is noted that a minimum translation speed of near or over 10 km h^{-1} on 8 August is also obtained in the control runs of several previous studies on Morakot using NCEP analyses (e.g., Liang et al. 2011; Huang et al. 2011; Yen et al. 2011).

Thus, the robustness of our predictions with the ECMWF YOTC fields is confirmed and the changes in LH asymmetry indeed account for most of the differences in translation speeds in Fig. 15 (and Tables 3, 5). It is therefore concluded that the track of Morakot in the first 12 h upon leaving Taiwan was indeed influenced by the LH effect associated with asymmetric rainfall, such that it moved more slowly than might have been expected from the steering effect (Fig. 7).

b. *Steering flow analysis*

Chien and Kuo (2011) analyzed the evolution of the mean ambient (steering) flow of Morakot inside an annulus between 300 and 700 km at five levels between 700 and 300 hPa (every 100 hPa) using the 0.25° × 0.25° ECMWF YOTC analyses. Whereas the averaged steering flow was from the east and was weakening prior to 0000 UTC 8 August, the flow then changed to be from the south by 0000 UTC 9 August (their Figs. 13 and 14a,b), which is consistent with the track of Morakot (also Wu et al. 2011; Liang et al. 2011). During the transition period on 8 August, the steering flow changes occurred mainly at 300–400 hPa, where weak northerly-to-northeasterly winds were analyzed (also Fig. 18). Since a southerly flow of about 9–18 km h^{-1} was maintained at 500–700 hPa (Chien and Kuo 2011), the deep-layer-averaged mean flow was then from the south (cf. Fig. 18).

Similar calculations of the 700–300-hPa mean flow as in Fig. 18 (over a circular area within 700 km) have been made using ECMWF YOTC, ECMWF TOGA (1.125° × 1.125°), and NCEP analyses (Fig. 19). In agreement with Chien and Kuo (2011), the deep-layer mean flow shifted from easterly to southerly on 8 August (Fig. 19a), and reached a minimum speed around 0000 UTC 8 August (Fig. 19b). Note that the estimated mean flow speeds vary from about 7.2 km h^{-1} at 0600 UTC 8 August (cf. Fig. 18) to over 11.5 km h^{-1} at 0000 UTC 9 August. However, the translation speed of Morakot was even smaller during this period (Figs. 19a,b, cf. Fig. 1); that is, the mean flow speed averaged over 0600–1800 UTC 8 August was about 9 km h^{-1} and the translation speed of Morakot was only about 5.5 km h^{-1}. These calculations are consistent with the tests R01–R04 (Table 3, Figs. 15a–c), in which the TC translation speed is reduced to 5 km h^{-1} after 0000 UTC 8 August with the full moisture but was near 10 km h^{-1} with limited moisture. As

TABLE 4. As in Table 3, but for the summary of TC translation speeds (1 km h^{-1} = 0.28 m s^{-1}) and directions determined using upper-level centers near 6.1 km in R01–R04.

	0000–1200 UTC 8 Aug (12 h)		1200–2400 UTC 8 Aug (12 h)		0000–2400 UTC 9 Aug (24 h)	
Expt	Speed (km h^{-1})	Direction (°)	Speed (km h^{-1})	Direction (°)	Speed (km h^{-1})	Direction (°)
R01	4.70	10	11.38	347	10.84	324
R02	7.40	360	11.29	317	11.19	335
R03	3.79	347	11.02	337	10.96	332
R04	3.79	13	13.80	331	11.60	343

TABLE 5. As in Table 3, but for the summary of TC translation speeds (1 km h^{-1} = 0.28 m s^{-1}) and directions during two 12-h time periods on 8 Aug for the sensitivity tests J01–J03 and N01–N03.

	0000–1200 UTC 8 Aug		1200–2400 UTC 8 Aug	
Expt	Speed (km h^{-1})	Direction (°)	Speed (km h^{-1})	Direction (°)
J01	9.28	355	10.04	317
J02	11.88	339	12.74	291
J03	13.80	331	8.53	276
N01	8.99	338	7.53	317
N02	13.24	352	9.48	321
N03	14.39	315	6.99	302

noted earlier, the differences in speed among J01–J03 and N01–N03 are also close to 5 km h^{-1}, although J01 and N01 admittedly capture less of the slow motion using JMA and NCEP analyses as ICs/BCs, respectively.

c. Diagnostics on TC motion

In this section, further diagnosis on the TC motion in the sensitivity tests will be explored based on kinematics of low pressure systems. Consider first the TC vortex structure near 2.1 km (level 9) during 0000–1200 UTC 8 August in R01 (CTL2) and R03 (Fig. 20). For the 25% reduced water vapor test (R03), the model vortex structure shows a steady degradation with time. Even though the integration is only 12 h, such a weakening is anticipated since the latent heat release has been greatly reduced and thus the vertical coupling mechanism is almost missing in the model as discussed. Thus, a comparison between the vortices in R01 and R03 can illustrate the reduced LH effect on the TC motion.

In a quasi-Lagrangian (QL) frame following the movement of a pressure system, the total derivative $\delta Q/\delta t$ of an arbitrary quantity Q can be expressed as

$$\frac{\delta Q}{\delta t} = \frac{\partial Q}{\partial t} + \mathbf{C} \cdot \nabla_h Q, \tag{1}$$

where $\partial Q/\partial t$ is the local tendency of Q in a fixed (Cartesian) frame, $\mathbf{C} = (c_x, c_y)$ is the motion vector in the x–y plane at origin of the QL frame, and ∇_h is the horizontal gradient operator. For a low pressure center (such as a TC) where $\nabla_h p = 0$ (or near 0), let $Q = \nabla_h p$ and $\partial^2 p/\partial x \partial y$ can be assumed negligible. Substituting these relationships into Eq. (1), $\mathbf{C}$ can be solved as

$$c_x = \frac{\partial(\delta p/\delta t - \partial p/\partial t)/\partial x}{\partial^2 p/\partial x^2}, \qquad c_y = \frac{\partial(\delta p/\delta t - \partial p/\partial t)/\partial y}{\partial^2 p/\partial y^2}. \tag{2}$$

Thus, Eq. (2) can be used to diagnose the motion of a TC, such as Morakot, based on simple kinematics.

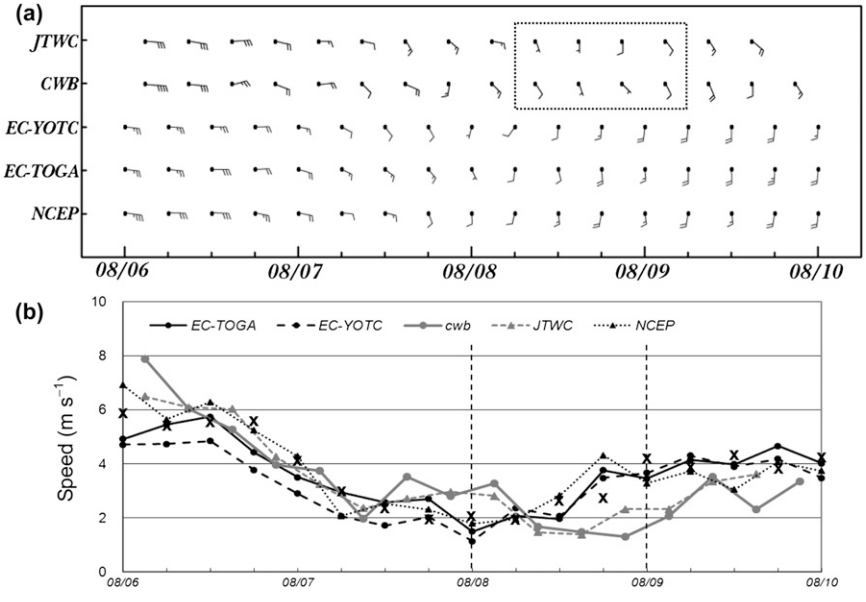

FIG. 19. (a) Mean flow [full (half) barbs are 2 (1) m s^{-1}] from 300 to 700 hPa over a circular area of radius 700 km from the three datasets compared with the motion vectors from center positions of Morakot from two operational agencies (JTWC and CWB) at 6-h intervals during 0000 UTC 6–10 Aug 2009. The 8–9 Aug period when Morakot clearly moved slower than the mean flow is indicated by a dotted box. (b) As in (a), but the flow and moving speeds are plotted as curves. Mean steering flow speeds obtained by Chien and Kuo (2011) are marked by crosses in (b).

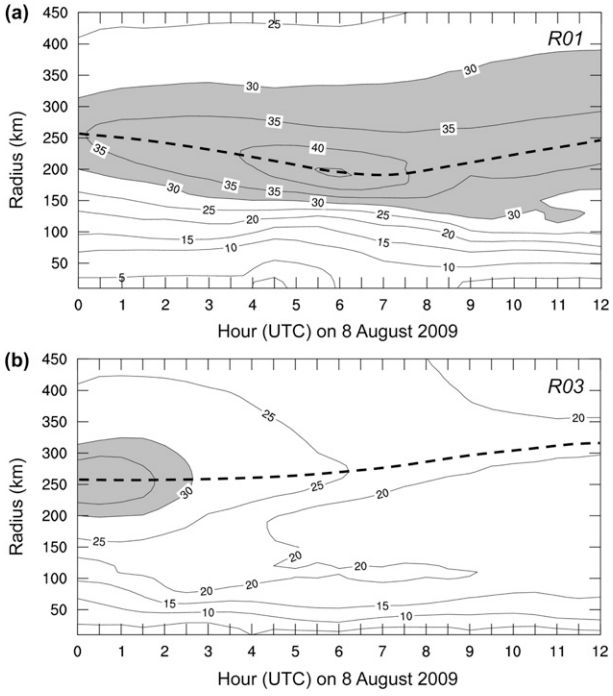

FIG. 20. Distribution of azimuthally averaged wind speed (m s^{-1}) at a height near 2.1 km with respect to radius from TC center during 0000–1200 UTC 8 Aug 2009 in sensitivity test (a) R01 and (b) R03. Thick dashed curves depict the radius of maximum wind.

Such a diagnosis is performed here for the R01 and R03 tests for all height levels. The results averaged through the layer of 3–7 km and over 0000–1200 UTC 8 August, and aggregated from 3- to 30-km horizontal resolution to smooth out cloud-scale features are shown in Fig. 21.

For the full moisture R01 test (Fig. 21a), the horizontal Laplacian of p ($\nabla_h^2 p = \partial^2 p/\partial x^2 + \partial^2 p/\partial y^2$) within about 200 km from the TC center is mostly positive as expected. The p tendency difference ($\delta p/\delta t - \partial p/\partial t$) of about 25 Pa $(30\ \text{min})^{-1}$ over 500 km in the numerator in Eq. (2) has a clear dipole structure with positive values to the north-northwest and negative values to the southeast of the TC center. As Eq. (2) is intended to apply at (or near) the TC center, the (smoothed) diagnostic motion vectors are only plotted within a radius of 180 km. These vectors are generally pointed toward the north-northwest at 3.6–10.8 km h^{-1}, with a mean value of 4.8 km h^{-1} toward 341° (Fig. 21a). For the 50% reduced moisture test in R03 (Fig. 21b, cf. Figs. 16c, 17a), the values of $\nabla_h^2 p$ around the TC center are somewhat reduced as expected from Fig. 20b. However, the p tendency difference becomes larger [about 45 Pa $(30\ \text{min})^{-1}$ over 500 km], so the motion vectors are significantly larger (roughly 7.2–18 km h^{-1}) toward the northwest, with a mean value inside 180 km of 11.2 km h^{-1} toward 319°. This faster motion in R03 is mainly caused by a nearly doubled gradient of p tendency difference in magnitude, especially near the TC center. Since the LH effect just to the southeast of the center in R01 decreases $\partial p/\partial t$ (becoming more negative) and raises the p tendency difference (to near and above zero), this eventually lowers the gradient of $\delta p/\delta t - \partial p/\partial t$ near the center (cf. Fig. 21a). The larger vector in R03 is also partially due to the weaker values of $\nabla_h^2 p$ surrounding the TC center.

The difference between the two (mean) motion vectors in Figs. 21a,b is 5.8 km h^{-1} at 125°, that is, toward the southeast or the rear of the TC, which is considered to mainly correspond to the (asymmetric) LH effect due to the rainfall differences shown in Fig. 17a. Although not examined here, it is likely that the slow background flow during this period (e.g., Chien and Kuo 2011; Wu et al. 2011) may have enhanced the impact of the asymmetric diabatic LH effect as suggested by Chan et al. (2002). Overall, the kinematic diagnosis of the TC motion difference in Fig. 21 is quite consistent with the asymmetric LH effect hypothesis (Fig. 7), as well as with the results of sensitivity tests (sections 3 and 4a) and steering flow analysis (section 4b).

5. Summary and conclusions

Typhoon Morakot (TY0908) struck Taiwan in early August 2009, and it brought extreme rainfall of almost 3000 mm in southern Taiwan and caused the worst damage in the past 50 yr. Typhoon–monsoon flow interactions with mesoscale convection, the water vapor supply by the monsoon flow, and the slow moving speed of the storm are considered to be the main reasons for the record-breaking rainfall. In particular, the unusually slow translation speed (only about 5 km h^{-1}) toward the north-northwest of Morakot on 8 August upon leaving Taiwan was an important key factor for the extreme rainfall, as the rain was also the heaviest during this period. Since a persistent asymmetric rainfall pattern to the south–southeast of Morakot existed due to the interaction of the typhoon circulation with the monsoon flow (and vertical wind shear), the slow speed on 8 August is hypothesized to have a contribution from the latent heating effect associated with the asymmetric rainfall. Sensitivity tests with the CReSS model have been used to test this hypothesis.

Using the ECMWF YOTC gridded analyses at 0.25° and 6-h resolution as ICs/BCs, the CReSS model with a grid size of 3 km and 50 levels is highly skillful in capturing the structural characteristics and overall evolution of Morakot during 6–10 August 2009, including its slow speed on 8 August. The rainfall simulation over Taiwan also compares favorably with rain gauge data in both amount and distribution. Sensitivity tests with

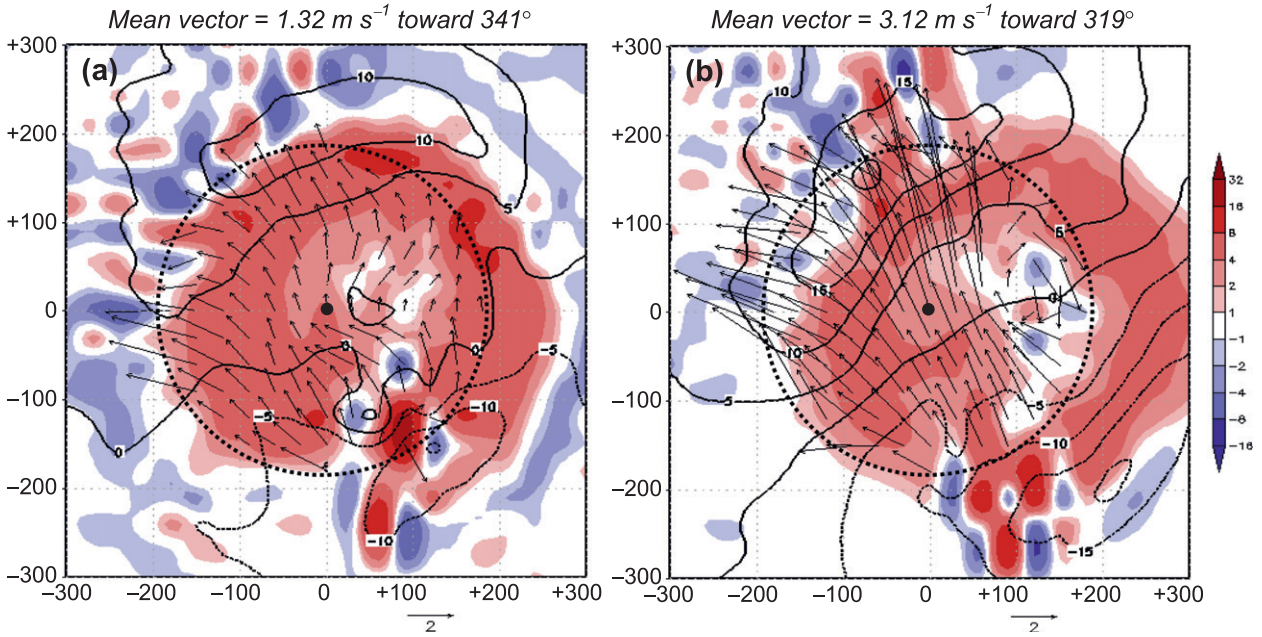

FIG. 21. The 3–7-km vertically averaged Laplacian of p (10^{-8} Pa m^{-2}; color, scale on right), difference in p tendency in QL minus fixed frame [$\delta p/\delta t - \partial p/\partial t$; Pa (30 min)$^{-1}$; thick contours, dashed for negative values], and diagnostic TC motion vectors $\mathbf{C} = (c_x, c_y)$ (m s^{-1}, reference vector plotted at bottom) after averaging within a radius of 180 km (dotted circle) and over the period 0000–1200 UTC 8 Aug 2009 for the (a) R01 (CTL2) and (b) R03 tests. These vectors are plotted in QL frame (x and y axes in km), and the TC center is depicted by a solid circle at the origin. All variables have been aggregated from 3- to 30-km resolution on x–y plane to remove small-scale features, and the motion vectors are further smoothed by a nine-point smoother 3 times.

different moisture content (100%, 50%, 25%, and 0%) and with different Taiwan terrain heights (100%, 50%, and 0%) have been carried out for the critical postlandfall period of 0000 UTC 8–10 August. These tests have consistent discernible differences in the motion of Morakot during 0000–1200 UTC on 8 August due to the moisture content variations. Specifically, the storms with 100% moisture content (and full LH effect) move the slowest (~5 km h^{-1}) and those with reduced moisture (25% and 0%) move much faster (~10 km h^{-1}). Thus, these tests suggest that the asymmetric LH effect contributed to a slowdown of Morakot by about 5 km h^{-1} (or as much as 50%). A small portion of the slowdown may be attributable to a weakening in the vertical coupling mechanism and subsequently a faster advection by the strong southerly flow at low levels. The speed differences and the robustness of our results are further confirmed through additional tests using JMA regional analyses and NCEP final analyses for the ICs/BCs.

Analysis of the mean ambient (steering) flow within a radius of 700 km of Morakot is carried out from three datasets (ECMWF YOTC, ECMWF TOGA, and NCEP). In general agreement with the results of Chien and Kuo (2011), the estimated 700–300-hPa deep-layer mean flow was indeed slow on 8 August, but it still averaged about 9 km h^{-1}. Thus, the synoptic steering flow exceeded the typhoon translation speed by approximately 4–5 km h^{-1} during the postlandfall period, when the extreme rainfall occurred in southern Taiwan. The speed reduction calculated for the LH sensitivity tests is in general agreement with this difference between the synoptic steering speed and the observed typhoon translation speed and is supported by a diagnosis of TC motion based on simple kinematics of pressure systems. When Morakot moved farther away and the asymmetric heating decreased, the track differences among the tests become smaller. Reduced topography sensitivity tests have a smaller effect on the track compared to the moisture tests. The rainfall was reduced in the southern CMR, but the overall asymmetrical rainfall pattern that arises from the interaction and convergence between typhoon circulation and monsoon flow was maintained.

This study emphasizes the potential contribution of asymmetric heating to the slowdown of typhoon motion in the presence of complex terrain or in a monsoon environment. Consequently, all processes related to latent heat release in the model, most importantly the cloud microphysics, must be accurately represented for a successful simulation (or prediction) of TC tracks, owing to nonlinear feedbacks between the TC track and the

rainfall distribution. Given the significant effects in the case of Morakot, more study is recommended since it is not uncommon for western North Pacific TCs to have asymmetric rainfall patterns.

Acknowledgments. The authors thank Prof. Russ Elsberry of the Naval Postgraduate School; Dr. Chris Landsea of the National Hurricane Center, National Oceanic and Atmospheric Administration; Dr. Eric Hendricks of the Naval Research Laboratory (NRL); and the anonymous reviewers for their constructive comments and suggestions. Valuable discussions with Prof. Kerry Emanuel of the Massachusetts Institute of Technology; Dr. Greg Holland of the National Center for Atmospheric Research; Prof. G. T.-J. Chen of National Taiwan University, Taiwan; and Prof. L. Wu of the Nanjing University of Information Science and Technology, China, are appreciated. Thanks also to the ECMWF YOTC project; to Dr. Lei Feng of the Taiwan Typhoon and Flood Research Institute (TTFRI) for providing Fig. 2; to the National Science and Technology Center for Disaster Reduction (NCDR) of Taiwan for providing the radar data used in Fig. 6; to NRL for making Fig. 5 available; and to Ms. S.-Y. Huang, Y.-W. Wang, T.-C. Lin, and Y.-W. Huang for their assistance throughout the course of this work. This study was supported jointly by the National Science Council of Taiwan under Grants NSC-99-2111-M-003-004-MY3, NSC-101-2625-M-003-001, NSC-98-2745-M-002-008-MY3, and NSC-100-2111-M-002-004-MY3 and by the U.S. Office of Naval Research under N62909-11-1-7096.

REFERENCES

Akter, N., and K. Tsuboki, 2012: Numerical simulation of Cyclone Sidr using a cloud-resolving model: Characteristics and formation process of an outer rainband. *Mon. Wea. Rev.,* **140,** 789–810.

Asselin, R., 1972: Frequency filter for time integrations. *Mon. Wea. Rev.,* **100,** 487–490.

Chan, J. C.-L., 1984: An observational study of the physical processes responsible for tropical cyclone motion. *J. Atmos. Sci.,* **41,** 1036–1048.

——, F. M. F. Ko, and Y. M. Lei, 2002: Relationship between potential vorticity tendency and tropical cyclone motion. *J. Atmos. Sci.,* **59,** 1317–1336.

Chang, C.-P., T.-C. Yeh, and J.-M. Chen, 1993: Effects of terrain on the surface structure of typhoons over Taiwan. *Mon. Wea. Rev.,* **121,** 734–752.

Chanson, H., 2010: The impact of Typhoon Morakot on the southern Taiwan coast. *Shore Beach,* **78** (2), 33–37.

Chen, T.-C., and Coauthors, 2010: The characteristics of radar-observed mesoscale rainbands of Typhoon Morakot (in Chinese). Scientific report on Typhoon Morakot (2009), H.-H. Hsu et al., Eds., National Science Council, 53–81.

Chien, F.-C., and H.-C. Kuo, 2011: On the extreme rainfall of Typhoon Morakot (2009). *J. Geophys. Res.,* **116,** D05104, doi:10.1029/2010JD015092.

Corbosiero, K. L., and J. Molinari, 2002: The effects of vertical wind shear on the distribution of convection in tropical cyclones. *Mon. Wea. Rev.,* **130,** 2110–2123.

——, and ——, 2003: The relationship between storm motion, vertical wind shear, and convective asymmetries in tropical cyclones. *J. Atmos. Sci.,* **60,** 366–376.

Cotton, W. R., G. J. Tripoli, R. M. Rauber, and E. A. Mulvihill, 1986: Numerical simulation of the effects of varying ice crystal nucleation rates and aggregation processes on orographic snowfall. *J. Climate Appl. Meteor.,* **25,** 1658–1680.

Fang, X., Y.-H. Kuo, and A. Wang, 2011: The impact of Taiwan topography on the predictability of Typhoon Morakot's record-breaking rainfall: A high-resolution ensemble simulation. *Wea. Forecasting,* **26,** 613–633.

Fiorino, M., and R. L. Elsberry, 1989: Some aspects of vortex structure related to tropical cyclone motion. *J. Atmos. Sci.,* **46,** 975–990.

Gall, R., 1976: The effects of released latent heat in growing baroclinic waves. *J. Atmos. Sci.,* **33,** 1686–1701.

Ge, X., T. Li, S. Zhang, and M. S. Peng, 2010: What causes the extremely heavy rainfall in Taiwan during Typhoon Morakot (2009)? *Atmos. Sci. Lett.,* **11,** 46–50.

Hendricks, E. A., J. R. Moskaitis, Y. Jin, R. M. Hodur, J. D. Doyle, and M. S. Peng, 2011: Prediction and diagnosis of Typhoon Morakot (2009) using the Naval Research Laboratory's mesoscale tropical cyclone model. *Terr. Atmos. Oceanic Sci.,* **22,** 579–594, doi:10.3319/TAO.2011.05.30.01(TM).

Hong, C.-C., M.-Y. Lee, H.-H. Hsu, and J.-L. Kuo, 2010: Role of submonthly disturbance and 40–50 day ISO on the extreme rainfall event associated with Typhoon Morakot (2009) in southern Taiwan. *Geophys. Res. Lett.,* **37,** L08805, doi:10.1029/2010GL042761.

Hsu, H.-H., and Coauthors, Eds., 2010: Scientific report on Typhoon Morakot (2009) (in Chinese). National Science Council, 192 pp.

Hsu, J., 1998: ARMTS up and running in Taiwan. *Väisälä News,* **146,** 24–26.

Huang, C.-Y., C.-S. Wong, and T.-C. Yeh, 2011: Extreme rainfall mechanisms exhibited by Typhoon Morakot (2009). *Terr. Atmos. Oceanic Sci.,* **22,** 613–632, doi:10.3319/TAO.2011.07.01.01(TM).

Ikawa, M., and K. Saito, 1991: Description of a nonhydrostatic model developed at the Forecast Research Department of the MRI. MRI Tech. Rep. 28, 238 pp.

Jou, B. J.-D., C.-S. Lee, M.-D. Cheng, L. Feng, and Y.-C. Yu, 2010: Analysis on the synoptic environment and rainfall characteristics of Typhoon Morakot (in Chinese). Scientific report on Typhoon Morakot (2009), H.-H. Hsu et al., Eds., National Science Council, 1–26.

Klemp, J. B., and R. B. Wilhelmson, 1978: The simulation of three-dimensional convective storm dynamics. *J. Atmos. Sci.,* **35,** 1070–1096.

Kondo, J., 1976: Heat balance of the China Sea during the air mass transformation experiment. *J. Meteor. Soc. Japan,* **54,** 382–398.

Kuo, H.-C., Y.-T. Yang, and C.-P. Chang, 2010: Typhoon Morakot (2009): Interplay of southwest monsoon, terrain, and mesoscale convection. *Int. Workshop on Typhoon Morakot (2009),* Taipei, Taiwan, National Science Council and National Applied Research Laboratories, 55–73.

Kuo, Y.-H., R. Reed, and Y. Liu, 1996: The ERICA IOP 5 storm. Part III: Mesoscale cyclogenesis and precipitation parameterization. *Mon. Wea. Rev.,* **124,** 1409–1434.

Liang, J., L. Wu, X. Ge, and C.-C. Wu, 2011: Monsoonal influence on Typhoon Morakot (2009). Part II: Numerical study. *J. Atmos. Sci.,* **68,** 2222–2235.

Lin, Y.-L., R. D. Farley, and H. D. Orville, 1983: Bulk parameterization of the snow field in a cloud model. *J. Climate Appl. Meteor.,* **22,** 1065–1092.

Louis, J. F., M. Tiedtke, and J. F. Geleyn, 1981: A short history of the operational PBL parameterization at ECMWF. *Workshop on Planetary Boundary Layer Parameterization,* Reading, United Kingdom, ECMWF, 59–79.

Mellor, G. L., and T. Yamada, 1974: A hierarchy of turbulent closure models for planetary boundary layers. *J. Atmos. Sci.,* **31,** 1791–1806.

Miller, C. A., and A. G. Davenport, 1998: Guidelines for the calculation of wind speed-ups in complex terrain. *J. Wind Eng. Ind. Aerodyn.,* **74–76,** 189–197.

Moncrieff, M. W., 2010: The multiscale organization of moist convection and the intersection of weather and climate. *Why Does Climate Vary?, Geophys. Monogr.,* Vol. 189, Amer. Geophys. Union, 3–26.

Mullen, S. L., and D. P. Baumhefner, 1988: Sensitivity of numerical simulations of explosive oceanic cyclogenesis to changes in physical parameterization. *Mon. Wea. Rev.,* **116,** 2289–2329.

Murakami, M., 1990: Numerical modeling of dynamical and microphysical evolution of an isolated convective cloud—The 19 July 1981 CCOPE cloud. *J. Meteor. Soc. Japan,* **68,** 107–128.

——, T. L. Clark, and W. D. Hall, 1994: Numerical simulations of convective snow clouds over the Sea of Japan: Two-dimensional simulation of mixed layer development and convective snow cloud formation. *J. Meteor. Soc. Japan,* **72,** 43–62.

Nguyen, H. V., and Y.-L. Chen, 2011: High-resolution initialization and simulations of Typhoon Morakot (2009). *Mon. Wea. Rev.,* **139,** 1463–1491.

Reynolds, R. W., N. A. Rayner, T. M. Smith, D. C. Stokes, and W. Wang, 2002: An improved in situ and satellite SST analysis for climate. *J. Climate,* **15,** 1609–1625.

Segami, A., K. Kurihara, H. Nakamura, M. Ueno, I. Takano, and Y. Tatsumi, 1989: Operational mesoscale weather prediction with Japan Spectral Model. *J. Meteor. Soc. Japan,* **67,** 907–924.

Tsuboki, K., and A. Sakakibara, 2002: Large-scale parallel computing of cloud resolving storm simulator. *High Performance Computing: 4th International Symposium,* H. P. Zima et al., Eds., Lecture Notes in Computer Science, Vol. 2327, Springer, 243–259.

——, and ——, Eds., 2007: *Numerical Prediction of High-Impact Weather Systems: The Textbook for the Seventeenth IHP Training Course in 2007.* Hydrospheric Atmospheric Research Center, Nagoya University, and UNESCO, 273 pp.

Waliser, D. E., and M. Moncrieff, 2007: Year of tropical convection—A Joint WCRP-THORPEX activity to address the challenge of tropical convection. *GEWEX News,* No. 2, International GEWEX Project Office, Silver Spring, MD, 8–9.

Wang, C.-C., and W.-M. Huang, 2009: High-resolution simulation of a nocturnal narrow convective line off the southeastern coast of Taiwan in the mei-yu season. *Geophys. Res. Lett.,* **36,** L06815, doi:10.1029/2008GL037147.

——, G. T.-J. Chen, and S.-Y. Huang, 2011: Remote trigger of deep convection by cold outflow over the Taiwan Strait in the mei-yu season: A modeling study of the 8 June 2007 case. *Mon. Wea. Rev.,* **139,** 2854–2875.

Wang, Y., and G. J. Holland, 1996: Tropical cyclone motion and evolution in vertical shear. *J. Atmos. Sci.,* **53,** 3313–3332.

Willoughby, H. E., 1992: Linear motion of a shallow-water barotropic vortex as an initial-value problem. *J. Atmos. Sci.,* **47,** 242–264.

Wu, C.-C., and Y.-H. Kuo, 1999: Typhoons affecting Taiwan: Current understanding and future challenges. *Bull. Amer. Meteor. Soc.,* **80,** 67–80.

——, T.-H. Yen, Y.-H. Kuo, and W. Wang, 2002: Rainfall simulation associated with Typhoon Herb (1996) near Taiwan. Part I: The topographic effect. *Wea. Forecasting,* **17,** 1001–1015.

Wu, L., and B. Wang, 2001: Effects of convective heating on movement and vertical coupling of tropical cyclones: A numerical study. *J. Atmos. Sci.,* **58,** 3639–3649.

——, J. Liang, and C.-C. Wu, 2011: Monsoonal influence on Typhoon Morakot (2009). Part I: Observational analysis. *J. Atmos. Sci.,* **68,** 2208–2221.

Yen, T.-H., C.-C. Wu, and G.-Y. Lien, 2011: Rainfall simulations of Typhoon Morakot with controlled translation speed based on EnKF data assimilation. *Terr. Atmos. Oceanic Sci.,* **22,** 647–660, doi:10.3319/TAO.2011.07.05.01(TM).